AD-A107 613 WASHINGTON UNIV SEATTLE DEPT OF ELECTRICAL ENGINEERING F/G 20/12
PHOTOACOUSTIC SPECTROSCOPY OF DIELECTRIC AND SEMICONDUCTING SOL--ETC(U)
SEP 81 S S YEE AFOSR-77-3120
UNCLASSIFIED AFOSR-TR-81-0747 NL

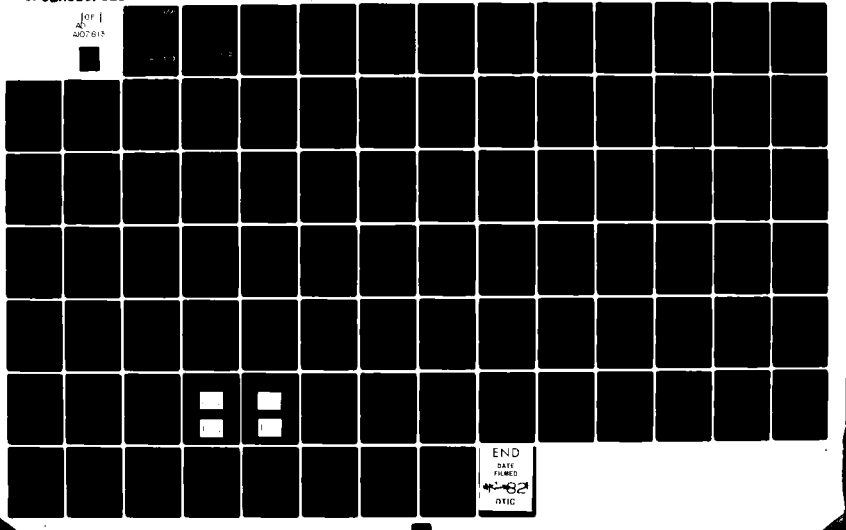

LEVEL

Final

12

Department of Electrical Engineering
College of Engineering
University of Washington
Seattle, Washington 98195

PHOTOACOUSTIC SPECTROSCOPY OF DIELECTRIC AND SEMICONDUCTING SOLIDS

Sinclair S. Yee

Principal Investigator

Final Report for Period 1 October 1976 - 30 September 1981

Grant Number AFOSR-77-3120

September 1981

Department of Electrical Engineering
University of Washington
Seattle, Washington 98195

Abstract

The recently developed techniques of solid state photoacoustic spectroscopy have been applied to the study of absorption processes in dielectric and semiconducting solids which are of interest in high power laser or electronic applications. The photoacoustic effect involves the irradiation, using a modulated light source, of a material in a closed cell. Incident photons which convert to heat in the sample by non-radiative processes result in temperature and pressure fluctuations in the coupling gas in the cell synchronous with the modulated source. Through the use of appropriate pulsed and chopped cw infrared and visible wavelength sources, these investigations have provided new information about a wide range of absorption effects including optical absorption in highly transparent materials, nonlinear absorption, localized defect characterization, spectroscopy of adsorbed surface impurities, and semiconductor absorption processes. The photoacoustic method has high sensitivity, good spatial and temporal resolution, and the ability to separately detect nonradiative processes, which have made it uniquely suited for these investigations.

REPORT DOCUMENTATION PAGE	READ INSTRUCTIONS BEFORE COMPLETING FORM
1. REPORT NUMBER AFOSR-TR- 81-0747 / 2. GOVT ACCESSION NO. AD-A107 613	3. RECIPIENT'S CATALOG NUMBER
4. TITLE (and Subtitle) PHOTOACOUSTIC SPECTROSCOPY OF DIELECTRIC AND SEMICONDUCTING SOLIDS	5. TYPE OF REPORT & PERIOD COVERED Final Scientific Report 01 Oct 76 - 30 Sep 81
	6. PERFORMING ORG. REPORT NUMBER
7. AUTHOR(s) Sinclair S. Yee	8. CONTRACT OR GRANT NUMBER(s) AFOSR-77-3120
9. PERFORMING ORGANIZATION NAME AND ADDRESS University of Washington Department of Electrical Engineering Seattle, Washington 98195	10. PROGRAM ELEMENT, PROJECT, TASK AREA & WORK UNIT NUMBERS 61102F 2301/A5
11. CONTROLLING OFFICE NAME AND ADDRESS AFOSR/NP Bolling AFB, DC Bldg. 410 Washington, DC 20332	12. REPORT DATE Sept 1981
	13. NUMBER OF PAGES 84
14. MONITORING AGENCY NAME & ADDRESS(if different from Controlling Office)	15. SECURITY CLASS. (of this report) UNCLASSIFIED
	15a. DECLASSIFICATION DOWNGRADING SCHEDULE

16. DISTRIBUTION STATEMENT (of this Report)

Approved for public release; distribution unlimited

17. DISTRIBUTION STATEMENT (of the abstract entered in Block 20, if different from Report)

18. SUPPLEMENTARY NOTES

19. KEY WORDS (Continue on reverse side if necessary and identify by block number)

20. ABSTRACT (Continue on reverse side if necessary and identify by block number)

The recently developed techniques of solid state photoacoustic spectroscopy have been applied to the study of absorption processes in dielectric and semiconducting solids which are of interest in high power laser or electronic applications. The photoacoustic effect involves the irradiation, using a mojulated light source, of a material in a closed cell. Incident photons which convert to heat in the sample by nonradiative processes result in temperature and pressure fluctuations in the coupling gas in the cell synchronous with the modulated source.

DD FORM 1 JAN 73 1473 EDITION OF 1 NOV 65 IS OBSOLETE

UNCLASSIFIED

SECURITY CLASSIFICATION OF THIS PAGE (When Data Entered)

Through the use of appropriate pulsed and chopped cw infrared and visible wavelength sources, these investigations have provided new information about a wide range of absorption effects including optical absorption in highly transparent materials, nonlinear absorption, localized defect characterization, spectroscopy of absorped surface impurities, and semiconductor absorption processes. The photoacoustic method has high sensitivity, good spatial and temporal resolution, and the ability to separately detect nonradiative processes, which have made it uniquely suited for these invesrigations.

Table of Contents

Section I

INTRODUCTION

The initial phase of the photoacoustic spectroscopy project discussed in this report is entitled "Photoacoustic Spectrometer for Investigating High Power Laser Window Materials" and was concerned with the development of a CO_2 laser photoacoustic instrument to characterize optical absorption in high power laser window and window coating materials. That phase of the project was completed with the period ending 30 September 1979. The second phase, which began 1 October 1979, was concerned with the extension of the window material absorption studies to other scientific applications of tunable infrared laser and visible light photoacoustic spectroscopy to solids and is entitled "Photoacoustic Spectroscopy of Dielectric and Semiconducting Solids." The research during the yearly period ending 30 September 1981 was concerned with (1) analysis and reporting of results for work with adsorbed surface impurities, (2) with modifications to the apparatus and design and construction of additional electronics for the infrared spectrometer, and (3) measurements and calculations involving visible wavelength spectroscopy of semiconductors. Research during this final period is described in Sections VI and VII of this report.

The interaction of radiation with matter and, in particular, the interaction of light with solids comprise fundamentally important phenomena which also have considerable practical importance in many technological areas including the development of high power laser window and window coating materials and the determination of photoelectronic

properties of semiconductors. The main scientific approach in the work here employs the photoacoustic effect, in which an acoustic signal is produced in a material during irradiation with a modulated light source, and which is directly associated with photon-phonon conversion and subsequent nonradiative decay processes in the solids. The central objective of this work is to obtain new information about, and to investigate physical models of, a wide range of absorption effects associated with light and laser interactions with solids. Specifically of interest are (1) spatial and chemical characterization of localized absorbers, such as inclusions or metallic impurity clusters in highly transparent materials, (2) the measurement of absorption spectra of impurities, especially infrared absorption properties of contaminants and adsorbed gases at surfaces of transparent solids, (3) detection of nonlinear absorption processes as are associated with laser induced damage in semiconductors, and (4) visible wavelength absorption processes in selected semiconductors.

The original description of the photoacoustic effect, that is, the production of an acoustic signal when modulated light is incident on a material in an enclosed cell, was given by Alexander Graham Bell in 1880.[1] Bell discovered that, in addition to the changes produced in the electrical properties of a selenium receiver element which was used for modulated light, an acoustic signal could be detected directly. The light was incident on an interior surface from which air was lead through a tube directly to the ear. The correct interpretation of this effect for solid samples has been presented only very recently,[2,3,4] although the effect has been understood and applied in studies of trace impurities in gases for many years.

The conventional application of the photoacoustic effect to the study of solids involves placing the sample in a sealed enclosure which is filled with a transparent gas. The sample is then irradiated through a transparent window in the cell with a chopped monochromatic or tunable light source for which the sample is at least partially absorbing. Photons absorbed by the sample and converted to heat give rise to temperature fluctuations, which result in heat conduction to a gas boundary layer adjacent to the sample, which in turn produces pressure fluctuations in the gas at an acoustic frequency corresponding to the chopping frequency of the source. In this experimental configuration, a lock-in amplifier having a tuned signal stage is used to detect the root-mean-square amplitude of the fundamental component of the acoustic signal, since this quantity may be compared with the results of theoretical calculations based on heat flow in the sample, gas, and window regions of the cell as discussed below.

Other experimental arrangements are possible, such as the use of a pulsed rather than a chopped source[5] or the detection of stress waves directly in the sample,[6] and can be applied when they present special advantages. An example of a useful modification for a relatively strongly absorbing sample is to use a pulsed source with a low repetition rate, rather than a chopped cw source, in order to limit local heating effects which could result in undesirable thermally induced changes in the absorption properties of the sample.

A simple model corresponding to a frequently used cylindrical photoacoustic cell configuration consists of the external air, windows, sample, and coupling gas regions. The microphone is connected to the interior gas region to detect the photoacoustic signal. The mathematical procedure for solving this problem for the one-dimensional case is to write the

thermal diffusion equations for the external, window, and sample regions and the hydrodynamic equation for the gas region of the cell. The solutions for the temperatures in the different regions are characterized by oscillating and exponentially decaying factors in general, with the addition of an acoustic (adiabatic) mode in the gas. Using the boundary conditions for temperature, heat flux, and gas velocity, it is possible to determine the unknown constants in the general solutions and to obtain predictions for the absolute value of the pressure oscillation (the photoacoustic signal). Details of such calculations will be discussed in Section II.

Some theoretical and experimental results[4,7] which are useful for the following discussions can be given briefly here. For the case of transparent solids, it can be derived that a sample having only a surface absorption will have a photoacoustic signal proportional to f^{-1} and that a sample having only a bulk absorption will have a signal proportional to $f^{-3/2}$, where f is the chopping frequency. Additionally, a bulk signal has a phase lag of 45° relative to that of a surface signal. For the case of nontransparent solids, the bulk absorption contribution to the photoacoustic signal will have a less strong frequency dependence than $f^{-3/2}$ due to the location of the initial heat distribution closer to the surface than is the case for a transparent material, for which the initial heat distribution is essentially constant through the depth of the sample.

A thermal wave is altered as it travels through a solid by a factor $\exp[-(j\frac{2\pi fc}{K})^{1/2}L]$, such that contributions to a detected signal from deeper than the thermal diffusion length are negligible,[8] where the thermal diffusion length is defined by $L_{th} = (\frac{K}{\pi fc})^{1/2}$ and where K and c are the

thermal conductivity and the specific heat per unit volume, respectively. Note that the thermal diffusion length decreases with increasing chopping frequency.

Section II

THEORY

1. Introduction

Several researchers have introduced different approaches for the calculation of photoacoustic signals. However the method of Parker[3] has been found to be accurate and relatively simple to apply. In this section, which is based on an extension by Lee[9] of Parker's technique, the physical model of photoacoustic phenomena is reviewed, and an extended calculation is presented. Finally, the chopping frequency response is discussed.

2. Physical Model

Figure 1 introduces the cell geometry pertinent to the generation of photoacoustic signals. The sample (region 4) is placed inside a closed cell containing air (region 3) or other gas which is transparent to the incident radiation. A backing plate (region 5) is used to support the sample and is assumed to have good thermal contact with the sample. As a matter of fact, in many cases, the samples are surface layers grown on the backing plate. The cell is then illuminated by chopped monochromatic light, as shown in the figure. In our theoretical analysis, we assume that optical absorption of the chopped light takes place not only in the sample, but also in the window and the backing plate, although the optical absorption of the window is usually much smaller than that of the sample and backing materials. If the sample absorbs any of the energy incident on it, some energy level in the sample has thus been excited, and this energy level

must subsequently de-excite. There are two major mechanisms to account for the de-excitation of the absorbed light energy in the solid: part of the energy may be converted to light of different wavelengths through radiative recombination processes, and the rest is converted to heat by non-radiative processes. When the chopped light source is turned on for a while, after a short transient period, the temperature of the solids (sample, window and backing plate) assumes a steady state characterized by a constant plus a small amplitude fluctuation whose frequency is the same as that of the modulated light input. There is also a flow of heat energy from the solid to the solid-gas interface by means of diffusion and therefore, the gas on the boundary layer experienced a temperature variation of the same frequency. Two mechanisms are responsible for the heat transfer within the gas: (1) the "thermal mode" corresponds to thermal diffusion in the gas, attenuates very fast, and is not so important. (2) The "acoustic mode" (or "propogation mode") corresponds to a nearly adiabatic process, generates a pressure wave which is detected by a microphone and referred to as the photoacoustic signal. Physically, the generation of the photoacoustic signal can be explained as follows: Because of the heat transfer across the solid-gas interface, the gas within a diffusion length adjacent to the sample surface would have the same temperature variation as the solid. Since the enclosed gas obeys the ideal gas law (at least to the first approximation), the expansion and contraction of the boundary layer gas due to the temperature change serves as a driving piston to the remaining portion of the gas in this cell and generates the pressure wave.

The temperature variation in the gas and thus the photoacoustic signal depends on both the optical absorption characteristics and

thermal properties of the sample. Knowing the optical and thermal properties of a solid, the photoacoustic signal can be calculated for that solid. Conversely, for a solid with known thermal properties, it is also possible to deduce the optical absorption characteristics from the measured photoacoustic signal. The relationship between optical absorption and photoacoustic pressure is derived from the solution of heat transfer equations with appropriate boundary conditions.

3. Mathematical Formulation

As mentioned above, the temperature variation of the solid-gas system can be calculated by solving heat transfer equations. Then the pressure variation, or the photoacoustic signal, can be determined from the temperature variation through thermodynamic relations. To simplify the mathematical calculation, some assumptions are made. These assumptions are:

1. Reflection loss of the incident light on window and sample surfaces is neglected.

2. The gas in the cell is non-absorptive to the incoming light beam.

3. The light intensity decays exponentially throughout the sample. Thus, the heat energy absorbed per unit time and length at a point a distance L from the surface of the sample is proportional to $\beta \exp(-\beta L)$, where β is the optical absorption coefficient.

4. The measured signal is independent of the diameter of the incident beam: the cell diameter may be any convenient size if it is filled by the beam. If the diameter of the beam is reduced, the intensity may be increased by focusing the beam but the irradiated volume

is decreased proportionally. These two factors cancel each other, so the measured signal is independent of the beam diameter.

5. We also assume that the gas chamber is sufficiently thin (compared with the acoustic wavelength) so that the heat flows primarily in a one-dimensional manner between windows. We neglect any heat flow from the sample to the cell walls. This assumption and assumption 4 enable us to solve this problem as a one-dimensional problem.

Accepting these assumptions, we are ready to set up the appropriate equations and boundary conditions.

a. Heat Transfer Equations

In Figure 1, assuming window 2 is highly transparent to the incident light, the ac component of temperature, T_2, satisfies the thermal diffusion equation:

$$-K_2\frac{d^2T_2}{dx^2} + j\omega C_2T_2 = \alpha_2 I \ , \ \alpha_2 d_1 << 1 \qquad (1)$$

where K_2(cal/cm·sec·°K) is the thermal conductivity of region 2; C_2(cal/cm^3·°K) is the specific heat per unit volume; ω(sec^{-1}) is the angular chopping frequency; α_2(cm^{-1}) is the optical absorption coefficient, and I(W/cm^2) is the intensity of incident light. In region 4 and 5, temperature is determined by

$$-K_4\frac{d^2T_4}{dx^2} + j\omega C_4T_4 = \alpha_4 Ie^{-\alpha_4(x-L/2)} \qquad (2)$$

$$-K_5\frac{d^2T_5}{dx^2} + j\omega C_5T_5 = \alpha_5 Ie^{-\alpha_4 d_2}e^{-\alpha_5(x-L/2-d_2)} \qquad (3)$$

where K_4, C_4, α_4, (K_5, C_5, α_5) are thermal conductivity, specific heat, and absorption coefficient, respectively.

Neglecting gas viscosity, the thermal transport in the gas (regions 1, 3, 6) is governed by

$$j(K_g/\omega)\nabla^4 T_i+[C_{pg}+j(\frac{\gamma K_g}{\omega})]\nabla^2 T_i+k_0^2 C_{pg} T_i = 0,\ i=1,3,6 \qquad (4)$$

where K_g(cal/cm·sec·°K) is the specific heat per unit volume at constant volume; γ is the ratio of specific heats; and $k_0=\omega/C_0$, C_0 (cm/sec) being the velocity of sound in the gas. A complete derivation of equation (4) is presented under subsection c below.

The solutions of equations (1), (2), and (3) are, respectively

$$T_2(x) = A_2 e^{-k_2(x+L/2+d_1)}+B_2 e^{k_2(x+L/2+d_1)} \qquad (5)$$

$$T_4(x) = A_4 e^{-k_2(x-L/2-d_2)}+B_4 e^{k_4(x-L/2-d_2)} + \frac{\alpha_4 I}{-K_4\alpha_4^2+j\omega C_4} e^{-\alpha_4(x-L/2)} \qquad (6)$$

$$T_5(x) = A_5 e^{-k_2(x-L/2-d_2-d_3)}+B_5 e^{k_2(x-L/2-d_2-d_3)} + \frac{\alpha_5 I}{-K_5\alpha_5^2+j\omega C_5} e^{-\alpha_4 d_2-\alpha_5(x-L/2-d_2)} \qquad (7)$$

where $k_i = (j\omega C_i/K_i)^{1/2}$, i = 2, 4, 5.

The solution of equation (2-4) may be written as

$$T_i(x) = T_{i0} + T_{i1}\ ,\ i = 1, 3, 6 \qquad (8)$$

where T_{i0} is the "acoustic mode" satisfying

$$\nabla^2 T_{i0} + k_0^2 T_{i0} = 0\ ,\ i = 1, 3, 6 \qquad (9)$$

and T_{i1} is the "thermal mode" satisfying

$$\nabla^2 T_{i1} + k_g^2 T_{i1} = 0\ ,\ i = 1, 3, 6 \qquad (10)$$

where $k_g = (j\omega C_{pg}/K_g)^{1/2}$.

Therefore, considering only the outgoing wave, the temperature in region 1 and 6 can be written, respectively, as

$$T_1(x) = A_1 e^{jk_0(x+L/2+d_1)} + B_1 e^{k_g(x+L/2+d_1)} \tag{11}$$

$$T_6(x) = A_6 e^{-jk_0(x-L/2-d_2-d_3)} + B_6 e^{-k_g(x-L/2-d_2-d_3)} \tag{12}$$

and in region 3

$$T_3(x) = A_3 e^{-jk_0 x} + B_3 e^{jk_0 x} + C_3 e^{-k_g x} + D_3 e^{k_g x} \tag{13}$$

Then the photoacoustic pressure is (see subsection c)

$$p(x) = C_{pg} T_{3o} - j(\gamma-1)(\omega K_g / C_0^2) T_{31} \tag{14}$$

From this equation, it can be seen that the pressure variation has a linear relationship with temperature variation.

b. Boundary Conditions

In order to determine the unknown constants in the general solutions, appropriate boundary conditions must be satisfied. Temperature and heat flux must be continuous at all boundaries. That is

$$T_i = T_{i+1} \ , \ i = 1, 2, 3, 4, 5 \tag{15}$$

$$K_i \frac{dTi}{dx} = K_{i+1} \frac{dTi+1}{dx} \ , \ i = 1, 2, 3, 4, 5 \tag{16}$$

where $K_{1, 3, 6} = K_g$.

Since gas velocity

$$u = (j/\omega\rho_0)(dp/dx) = 0 \tag{17}$$

at each solid-gas boundary surface, we have

$$dp/dx = 0 \tag{18}$$

at $x = -L/2-d_1, -L/2, L/2, L/2-d_2+d_3$. Consequently, we have fourteen boundary conditions for fourteen unknown constants. Since the analytic solution of this set of equations is very complex, a computer program

was generated to solve for these constants.

c. Derivation of Equation (4)

i) Glossary of Symbols:

C, C_0	speed of sound, $C_0 \equiv [(\partial P/\partial \rho)_S]_0 = (K_s/\rho)_0$
Cp, Cv	specific heats at constant pressure, constant volume
f	frequency
k, k_0	phase constant = $\omega/c = 2\pi/\lambda$, $k_0 = \omega/c_0 = 2\pi/\lambda_0$
K	thermal conductivity
p; P_1	sound pressure; first-order sound pressure
p, P_0	total pressure, equilibrium pressure
s	specific entropy of unit mass
t	time
T	absolute temperature
$\vec{u}$	particle velocity
v	specific volume = ρ^{-1}
β	coefficient of thermal expansion = $\rho(\partial v/\partial T)_p = \frac{1}{V}\frac{\partial V}{\partial T}$
γ	ratio of specific heats = $Cp/C_v = (K_s/K_t)$
η	coefficient of shear viscosity
θ_1	first-order variational component of temperature
K_s; K_t	isentropic modulus (or inverse of isentropic compressibility, $K_s = (-\frac{1}{V}\frac{\partial V}{\partial P})_s^{-1}$ isothermal modulus (or inverse of isothermal compressibility, $K_t = (-\frac{1}{V}\frac{\partial V}{\partial P})_t^{-1}$
λ; λ_0	wavelength = C/f ; $\lambda_0 = C_0/f$
ρ, ρ_0; ρ_1	total, equilibrium densities, first-order density
ω	angular frequency = $2\pi f$

ii) The Exact Equations

The motions of a fluid medium that comprise sound waves are governed

by equations that include: (1) a continuity equation expressing the conservation of mass, (2) a force equation expressing the conservation of momentum and (3) a heat-exchange equation expressing the conservation of energy. These equations will first be presented in their exact form before approximations are made in formulating the linearized, or small-signal, acoustic equations.

(1) Equation of Continuity:

$$\frac{\partial \rho}{\partial t} + \nabla \cdot (\rho \vec{u}) = 0 \tag{19}$$

(2) Force Equation (or Navier-Stokes Equation)

For a nonviscous fluid, the conservation of momentum can be written as

$$\rho \frac{\partial \vec{u}}{\partial t} = \rho \vec{F} - \nabla P \text{ where } D(\ )/Dt = \partial(\ )/\partial t + \vec{u} \cdot \nabla,$$

denotes the "material derivative." A more symmetrical form in terms of the mass transport velocity $\rho\vec{u}$ is obtained if the continuity equation (19) is multiplied by $\vec{u}$ and added to the above equation, giving

$$\frac{\partial(\rho \vec{u})}{\partial t} + \vec{u}(\nabla \cdot \rho \vec{u}) + (\rho \vec{u} \cdot \nabla)\vec{u} = \rho \vec{F} - \nabla P \tag{20}$$

(3) Energy Relations

The conservation of energy requires that the following power equation be satisfied:

$$\rho C_v \left(\frac{\partial T}{\partial t} + \vec{u} \cdot \nabla T\right) + \frac{\rho(Cp-Cv)}{\beta} \nabla \cdot \vec{u} - \nabla (K \nabla T) = 0 \tag{21}$$

iii) The Small-Signal Acoustic Equations

The linearized, or small-signal acoustic equations can be obtained by replacing the dependent variables in (19), (20) and (21) by the sum of their equilibrium or zero-order values and their first-order variation components, and then form the separate equations that must be satisfied by the variables of each order.

$$\rho = \rho_0 + \rho_1 \quad , \quad T = T_0 + \theta_1$$

$$\nabla\rho = \nabla\rho_1 \quad , \quad \nabla T = \nabla\theta_1$$

$$P(\rho,T) = P_0(\rho_0, T_0) + P_1$$

$$P_1 = [(\frac{\partial P}{\partial \rho})_T]_0(\rho-\rho_0) + [\frac{\partial P}{\partial T})_\rho]_0(T-T_0)$$

$$= (K_T/\rho)_0\rho_1 + [-(\frac{\partial P}{\partial \rho}) + (\frac{\partial \rho}{\partial T})_\rho]_0\theta_1$$

$$= C_0^2/\gamma(\rho_1 + \beta_0\rho_0\theta_1)$$

$$\vec{u} = 0 + \vec{u}_1 \ , \ \nabla\cdot\vec{u} = \nabla\cdot\vec{u}. \qquad (22)$$

When the above relations are substituted in (18), (19), (20) and the equation of state (22), the first-order acoustic equations can be separated out in the form

$$\frac{\partial \rho_1}{\partial t} + \rho_0(\nabla\cdot\vec{u}_1) = 0 \qquad (19)'$$

$$\rho_0\frac{\partial \vec{u}_1}{\partial t} + \nabla p_1 = 0 \qquad (20)'$$

$$\rho_0 C_v\frac{\partial \theta_1}{\partial t} + \frac{\rho_0 C_v(\partial-1)}{\beta_0}(\nabla\cdot\vec{u}_1) - K\nabla^2\theta_1 = 0 \qquad (21)'$$

$$\rho_1 = \frac{C_0^2}{\gamma}(\rho_1 + \beta_0\rho_0\theta_1) \qquad (22)'$$

iv) The Steady-State Heat-Transport Equation

To find the steady-state heat-transport equation, let

$$\theta_1 = T_2 e^{j\omega T} \quad , \quad \rho_1 = \rho_1' e^{j\omega T}$$

$$P_1 = P_1' e^{j\omega T} \quad , \quad \vec{u}_1 = \vec{u}_1' e^{j\omega T}$$

and substitute these variables into (18)', (19)', (20)' and (22)'. Combine these four equations and eliminate ρ_1', P_1', and $\vec{u}_1'$, the steady-state

heat-transport equation is obtained as

$$j(k/\omega)\nabla^4 T_2+[Cp+j(\gamma K/\omega)k_0^2]\nabla^2 T_2+k_0^2 Cp T_2 = 0 \qquad (4)$$

4. Results

Some results of calculations for the dependence of the photoacoustic signal on various parameters are given in Figures 2 through 4. These figures illustrate the effects of cell length, sample thickness, and spatial distribution of absorbers. Note in Figure 2 the limiting magnitude of the photoacoustic signal of low frequencies as the thermal diffusion length in the gas becomes comparable to the length of the cell. In Figure 3 note the features in the calculated response curves associated with the thermal diffusion length reaching a value equal to the sample thickness. Figure 3 demonstrates the f^{-1} and $f^{-3/2}$ chopping frequency dependence for surface and bulk absorption, respectively.

Section III

HIGHLY TRANSPARENT SOLIDS

1. Introduction

A photoacoustic method has been applied to the quantitative measurement of optical absorption at 10.6 μm in coated and uncoated alkali halide samples having a spatially varying optical absorption[9,10,11]. Photoacoustic signals were measured as a function of the chopping frequency of a CO_2 laser source. The dependence of the signals on chopping frequency and an absolute electrical calibration of the cell were used to interpret the data. The results are in good agreement with laser calorimetry or infrared transmission measurements on the same samples. Signal fluctuations identified with thermal and source-coherence effects are reported and discussed. The experiments reported here confirm the utility of the photoacoustic technique in the general investigation of optical properties of highly transparent materials.

The experiments reported here are part of a general program of applying the photoacoustic method to the study of surface and bulk optical absorption in high power laser window materials. Efforts have included the development and verification of theoretical models of the photoacoustic effect.[12] The particular samples discussed here to illustrate the use of the photoacoustic method are representative of samples that might be encountered in laser applications and are not necessarily optimally suited for studies of intrinsic properties of the alkali halides. A related photoacoustic method which utilizes the elastic waves generated in the solid and detected by attached transducers is also discussed.[6]

2. Theoretical Background

Some effects important to work with highly transparent materials are discussed here to supplement the additional background material given in Section II of this report. Some reported data have shown a decrease in the photoacoustic signal at low chopping frequencies relative to that which is predicted by current theories.[8,13] Theoretical work including a treatment of the coupling of thermal and acoustic waves has also been reported.[14]

The existence of entrance surface and exit surface power level differences occurs in general for a light beam transversing a solid.[15] This is due to reflection with and without phase change, respectively, from an entrance and an exit surface of a window. The resultant fields can give large entrance/exit power level ratios as calculated from the Fresnel reflection coefficients. Just inside the surfaces of a window, a power ratio of:

$$\frac{P_{exit}}{P_{ent}} = \frac{4n^2}{(n+1)^2}$$

occurs, where n is the refractive index. Inside the cavity formed by two windows and just outside their inner surface a ratio of:

$$\frac{P_{ent}}{P_{exit}} = \frac{4}{(n+1)^2}$$

would be obtained, with this case being of interest for certain adsorbed gas systems. Such power level differences at the sites of localized absorbers will affect photoacoustic signal levels.

For highly transparent materials, interference effects can occur over large distances due, for example, to interaction of the front and back reflections of a window with an incident coherent light beam and to the

interaction of the reflected beams with each other. Long range coherence effects have been reported for transmitted power through a GaAs crystal.[16] Related effects can occur in a photoacoustic cell configuration used for transparent materials. The general behavior would be a two (or more) level signal with fluctuation between levels being produced by thermal expansion. There would be a tendency to remain in the low absorption state due to the faster expansion that occurs in a higher absorption state. In principle such interference effects could be utilized to separate surface and bulk absorption with very high resolution. The magnitude of possible fluctuations as expansion produces constructive or destructive interference at a localized absorption site would be comparable to the exit and entrance power level differences given above.

An important class of problems for which the photoacoustic signal has not yet been calculated theoretically is that of absorption by small inclusions in a transparent solid, including nonlinear thermal effects. This case would require a complete solution for the three dimensional heat flow, perhaps using the finite element method. Absorption by such defects has been recognized and examined in an analysis of damage processes in window materials.[17] In photoacoustic samples the relative magnitude of distance from a surface, distance between inclusions, diameter, thermal diffusion length in the inclusion, and thermal diffusion length in the transparent solid would be important. In some special cases, the qualitative behavior of the frequency dependence of the photoacoustic signal might be predicted using the bulk and surface frequency dependence results of the one dimensional theory.

3. Experiment

A block diagram of the experimental apparatus is shown in Figure 5, with additional details being given in Figure 23, in Section VI. The CO_2 laser is an Apollo Laser, Inc. Model 500 operating near 10.6 μm with a maximum output of 50 W cw. The laser has been modified by adding dielectric coatings to the front reflector to avoid the possibility of oscillation near 9.6 μm. The laser power supply is operated in a chopped mode using an external trigger voltage. The power meter is a Coherent Radiation, Inc. Model 201. The condenser microphone is a Brüel and Kjaer model 4134 followed by a Model 2619 preamplifier giving an overall sensitivity of 1 mV/μbar. The lock-in is a Princeton Applied Research Corp. Model HR-8, which has a tuned amplifier stage and which detects the root-mean-square value of the fundamental component of the photoacoustic signal.

The aluminum photoacoustic cell has a cavity of approximately 0.5 cm thickness and 1.27 cm diameter. It is formed by two windows clamped against gaskets, as shown in Figure 6. The acoustic signal in the cell is coupled to the microphone through a 13-gauge hypodermic needle; this arrangement permits the cell volume to be small relative to the size of the microphone. The cell has valves which permit purging or evacuating and backfilling with gases other than air, if needed.

The electrical calibration method is shown in Figure 7. An electrically heated device is mounted in the photoacoustic cell and, when excited with a square wave, produces acoustic signals similar to those that would be produced by optical absorption in a window. The electrical power input to this device is measured and provides an absolute calibration for the cell.[18] For a thin-film on an insulating substrate the device is an analog to a transparent window with a thin surface absorptance and is expected to have a signal proportional to f^{-1}. The calculated

signal is shown as a straight line in Figure 8. The actual signal is a factor of two less sensitive than calculated over much of the range and exhibits several acoustic resonances. The ratio of experimental to theoretical response shown in Figure 3 defines the frequency response of the apparatus and is used to correct measured photoacoustic data.

The simplest operating procedure is to rotate the cell slightly away from normal incidence to bring reflections away from the laser cavity and to exclude the possibility of interference effects. When possible, the front window is chosen to have a very low absorption, so that the photoacoustic signal generated there and its phase relative to the sample of interest can be neglected.

4. Results

In Figure 9 data for NaF films deposited by thermal evaporation are shown. Results are presented for measurements on films deposited on KCl and NaCl windows (samples Y and Z, respectively) just after removing from the evaporation system. Also shown is the increased absorption occurring in a film which was deposited on KCl and which was permitted to deteriorate with atmospheric exposure (sample X). The materials used where random cuttings of NaF crystals and #L-02505 laser windows from Harshaw Chemical Company. The system NaF on NaCl represents an example of a single layer antireflection coating material application, and NaF itself is of general interest as a possible substitute for the radioactive ThF_4 in multilayer coatings.[19]

In Figure 10 photoacoustic data for a set of five RbCl-doped KCl samples are shown. The samples were cut from material prepared by Harshaw Chemical Company for the Air Force Materials Laboratory and were used for a study of the precision of optical absorption measurements.[20] The data in

Figure 10 are signals obtained from pairs of windows mounted in the photoacoustic cell. Five sets of data were taken using different configurations of the windows, and the five equations representing total signals for pairs of windows were solved for the individual window signals in Figure 11. Prior to making the measurements shown in Figure 10 for these samples, they were etched in HCℓ, rinsed in ethanol and two isopropanol rinses, and dried with a hot air blower. This is a standard etching procedure for reducing the surface absorption.[20]

A preliminary experiment has been performed to examine entrance and exit field effects on relative photoacoustic signals. A pair of NaCl windows was chosen for which it had previously been determined that a rinse in isopropanol would produce a reduction of the photoacoustic signal level relative to that which occurred after allowing atmospheric exposure of the windows. Only one of these windows was then cleaned following exposure, giving an expected reduction in surface absorption of at least a factor of 2. The pair was then mounted in the photoacoustic cell and measurements made with both orientations of the cell. The higher absorber was first further from the source and then closer to it making that surface first an entrance surface and then an exit surface for the laser beam. A ratio of 0.76 was obtained for signals for the two orientations. The equations in the theory section above predict a ratio of:

$$\frac{S_1}{S_2} = \frac{\frac{4}{(n+1)^2} r + 1}{\frac{4}{(n+1)^2} + r}$$

for the case where the absorber is located just outside the surface and where r is the ratio of absorption levels of the two windows. For $r = 2$ we obtain $s_1/s_2 = 0.86$ from the equation given above with larger values for r giving smaller values of s_1/s_2.

In Figure 12 data are presented which show the fluctuation of a photoacoustic signal between two levels as a function of time. This fluctuation is believed to be due to thermal expansion and its effect on the existence of constructive and destructive interference of reflected beams either at the surface or at the site of a localized defect. The samples in this case were etched KCℓ windows. The cell was initially at or near normal incidence. Obtaining continuous data was impeded by the existence of changes in times comparable to the time required to adjust the lock-in. The broken arrows in Figure 12 represent rapidly increasing or decreasing signals. More slowly fluctuating bistable signals have been obtained at lower incident powers with the two levels having a signal ratio of about 2 in most cases. The latter part of the data in the figure shows the elimination of the fluctuation by a rotation of the cell away from normal incidence (by about 4.6°).

5. Discussion

The NaF films of Figure 9 have an absorptance in a range that can be detected in infrared transmission as well as photoacoustically. The depositions of the films were performed in a high vacuum system without multiple evaporation steps or other special measures to purify the starting material. The absorption in these films is probably dominated by hydroxyl ions incorporated in the film due to interaction of the NaF vapor with residual gases in the vacuum system. This conclusion is supported by the infrared transmission spectra which show large peaks near 3μ associated with the stretching mode of OH but which have only small peaks near 6μ where a bending mode peak due to HOH occurs. The absorptance near 10.6 μm is about 4% from the transmission spectra and is near the limit of sensitivity for that method. This is to be compared with an absorptance of about 6% deduced from the photoacoustic signal using its

electrical calibration. Note that the photoacoustic signal is several orders of magnitude above its detection limit.

The results for the KCl crystals shown in Figure 10 and 11 exhibit approximately the f^{-1} dependence expected for surface absorption or for absorbers located in the region close to the surface relative to the thermal diffusion lengths for the 10 to 100 Hz frequency range. The calculated results in the second column of Table 1 show the photoacoustic absorptance results based on the electrical calibration and a fitting of a f^{-1} curve to this frequency range.

An additional feature of the data are increases to higher slopes at particular frequencies above 100 Hz. The increase occurs at frequencies that correlate inversely with the absorptance level. A possible source of this effect is subsurface inclusions. A particle would have the frequency dependence of a bulk absorber for diffusion lengths shorter than its distance from the surface but would have the frequency dependence of a surface absorber for long diffusion lengths (and low chopping frequency). In a more general model including the thermal properties of inclusions, slope changes would be expected when the thermal diffusion length in the inclusion approached its size. A conducting inclusion, for example, would absorb heat initially at its surface. This heat would flow toward the center for a distance comparable to the thermal diffusion of the inclusion. At lower frequencies and larger thermal diffusion lengths the particle would reach a constant temperature in a chopping cycle and would begin to heat the surrounding solid and contribute to the normal photoacoustic signal. Another type of signal level change would be that associated with a thermal diffusion length in the solid approximately equal to the mean inclusion-separation distance. The heat flow should change from one dimensional at small f and large L_{th} to three dimensional at large f and small L_{th}.

It has been found that measurements for a particular sample are reproducible within about 5% if the positioning of the sample relative to the beam is maintained. Other effects exist which limit the accuracy of the results presented here and which might require adjustments to the results in a more exact analysis. These effects include (1) the power level corrections associated with multiple reflections and (2) background signal levels associated with absorption by gas in the cell and with true surface absorption due to adsorbed gas layers.

In Table I a comparison of photoacoustic and laser calorimetry results is presented. The photoacoustic results are $2xA_s$ where A_s is a f^{-1} dependent (surface) absorptance derived from the data in Figure 11. The laser calorimetry data is derived from the measurments made on the same crystals using the slope method.[20] Since optical absorption measurements on highly transparent materials can differ considerably for measurements performed in different apparatus on the same samples, the agreement of the photoacoustic data in Table I is considered to be satisfactory compared to the laser calorimetry results for the etched samples shown in the last column. The last two rows in the table are data for the high absorbtance crystals which had many macroscopic defects. These defects were associated with the high laser calorimetry absorptance results.[20] The group of data reported here were obtained by careful positioning of samples to place the best available portion of the sample surfaces at the center of the laser beam. Different positioning of such samples yielded absorptance values larger by a factor of about 5. The positioning method for the reported measurements was chosen to give data most representative of the crystals rather than of a particular strongly absorbing surface defect.

Some preliminary data had been obtained on the same KCl crystals using the same cell but different electronics and an unmodified laser.[10] The frequency dependence and fractional change with etching were comparable to the later reproducible results for these and other crystals. However, the absolute signal levels were lower by a factor of about 50. Since the present signal levels are reproducible, the cause of the discrepancy is not completely known. A contributing factor must be the repeated etching of the crystals which increases surface area and damage. Additionally, it is possible that any 9.6 μm radiation from the laser prior to its modification was able to desorb surface contaminants which are known to have a 9.5 μm absorption band.[21]

Some comments should be made regarding the different photoacoustic techniques now in use. The method using the elastic waves in the solid seems to provide a strong separation of surface and bulk signals, since they appear with different signs, due to the different transducer response to spherical and radial waves.[6] The frequency dependence is quite complicated, however, and has not been calculated in detail theoretically. It is also necessary to perform the energy calibration separately for the surface and the bulk for each sample.

The photoacoustic method applied in the present work has a well-understood frequency dependence of the photoacoustic signal even for fairly complex systems. In practice it sometimes becomes relatively difficult to extract bulk absorption from total absorption signals when surface absorption dominates, unless very low frequencies are employed. This conventional application of the photoacoustic method also seems to have the potential to detect point defects or inclusions separately from distributed surface absorption.

6. Conclusion

The use of an electrically calibrated photoacoustic cell provides a sensitive method of determining optical absorption properties of highly transparent solids including nonhomogeneous systems. Complicating reflection, interference and thermal effects can occur in the geometric cell configuration frequently used, but these effects can be controlled with appropriate experimental procedures. Such effects, particularly interference, are expected to be of value in the separation of bulk and surface absorption in addition to the method of separation possible using the chopping frequency dependence of the signal.

Applications of the photoacoustic technique to general materials would be aided by theoretical work in the area of three dimensional heat flow. In particular, the theory for inclusions having thermal and optical properties different from the host material would be a valuable addition to present calculations, which treat the one dimensional problem of an optical absorption coefficient that varies with distance from the surface of the sample.[12]

The experiments reported here and the satisfactory agreement obtained with the techniques of laser calorimetry or infrared transmission point to the value of the photoacoustic method in quantitative absorption studies. The high sensitivity, spatial resolution, and temporal resolution become especially advantageous for evaluating complex sample configurations.

Table I. Comparison of total absorptance as determined by the photoacoustic method and by laser calorimetry for RbCℓ-doped KCℓ crystals (see text).

Sample	Photoacoustic Absorptance Results	Laser Calorimetry Absorptance Results
D	6.0×10^{-4}	6.3×10^{-4}
E	8.2×10^{-4}	8.6×10^{-4}
A	8.8×10^{-4}	9.4×10^{-4}
C	10.2×10^{-4}	23×10^{-4}
B	11.0×10^{-4}	25×10^{-4}

Section IV

NONLINEAR ABSORPTION

A photoacoustic technique has been used to detect the onset of a nonlinear optical absorption effect, as the incident intensity is varied, in semiconductor samples irradiated by a pulsed CO_2 laser source operating near 10.6 μm.[22] The results are compared with existing studies of laser-induced surface damage in similar samples. The general applicability of the photoacoustic method to the detection of nonlinear or regenerative processes prior to inducing irreversible physical damage in the sample is discussed.

The experimental apparatus used here is similar to that described in a previous study[11] with the exceptions that the CO_2 laser source was operated in a repetitive pulsed mode for the present experiments rather than in a chopped cw mode and that an antireflection-coated germanium lens was added to focus the beam to higher intensities. Briefly, the apparatus consists of an Apollo Laser, Inc. Model 500 CO_2 laser operating near 10.6 μm with a maximum output of 50 W cw. The laser has been modified by adding dielectric coatings to the front reflector to avoid the possibility of oscillation near 9.6 μm. The condenser microphone is a Brüel and Kjaer Model 4134 followed by a Model 2619 preamplifier, giving an overall sensitivity of 1 mV/μbar. The photoacoustic cell enclosure is formed by windows or samples clamped against gaskets on the aluminum body of the cell and has dimensions of 0.5 cm thickness and 1.27 cm diameter. The acoustic signal is coupled to the microphone through a 13-gauge hypodermic needle. A block diagram of the experimental apparatus is shown in Figure 13.

In the conventional photoacoustic apparatus, a chopped cw source is used, and the signal is detected using a lock-in amplifier. Alternatively, a pulsed source and a different type of signal processing can be used, and this case has recently been discussed theoretically and applied experimentally.[5] In the present study a pulsed source was used to avoid an excessive temperature rise in the partially absorbing samples.

Experimental results for a 0.038 cm thick Cr-doped GaAs crystal sample are given in Figure 14. The data are plotted as the photoacoustic signal base-to-peak pulse height per unit irradiated area versus the relative incident power per unit irradiated area. A clear deviation from the initial low-intensity linear-absorption region is visible. Similar results have been obtained in other experiments using a 0.020 cm thick Si sample. The intensity variation in Figure 14 was produced by combinations of beam focusing and laser power changes; however, either method of intensity variation alone was capable of producing sufficient intensity change to reach the nonlinear absorption region. This application of a photoacoustic technique to detect nonlinear response in a semiconductor is related to a recently described method[23] involving electrical, rather than optical, excitation of a semiconductor sample in an acoustic cell.

Some additional results are presented in Figures 15 and 16 to indicate the type of response obtained for pulsed excitation as described above. Figure 15 presents examples of the waveform for a bulk and for a surface absorption case. Figure 16 presents data for the response for thin crystals of two different materials, GaAs:Cr and Si.

The deviation from the initial slope for the data presented in Figure 14 corresponds to an intensity level for the onset of a nonlinear absorption of about 1.3 kW/cm^2 for the peak beam intensity of a gaussian beam. The calibration for this intensity level is based on transmission

measurements through apertures. The onset intensity given above may be compared with experimental results on the order of kW/cm^2 reported for a recent study of semiconductor surface damage using 0.15 to 0.18 second exposures to a cw CO_2 laser.[4] The accuracy of absolute intensity levels in these photoacoustic experiments, as in other similar experiments, is about 40% and is limited by the measurement of the incident beam size and its spatial distribution. The uncertainty in the relative intensity as plotted in Figure 14 is about 10%. The onset intensity obtained in this work is considered to be compatible with the existing experimental results referenced above for irreversible surface damage of semiconductor samples using a cw CO_2 laser source.

The photoacoustic data and theory presently available do not distinguish between the existence of a proposed surface-initiated parametric instability[24] and other possible types of localized heating. The effects reported here are not, however, attributable to thermally induced changes in the bulk absorption coefficient, since a limited pulse energy was used. It is expected that experiments with larger source intensity ranges, variable pulse lengths, and an appropriate series of independently characterized semiconductor samples would yield information related to fundamental causes of the damage mechanism.

In conclusion, a procedure has been described for detecting nonlinear absorption processes using a photoacoustic technique, and an example of its application has been given. The commonly used procedure in laser-induced damage studies of semiconductor or dielectric materials is to produce physical damage that is difficult to quantify. The technique described here permits the detection of the onset of nonlinear absorption or the measurement of the progression of regenerative processes at pre-damage levels.

Section V

LOCALIZED ABSORPTION

Recently the detection of the surface and subsurface structure of silicon nitride ceramics by laser photoacoustic spectroscopy has been demonstrated[25], and a modification of an acoustic microscope for photoacoustic analysis has been reported.[26] A theoretical calculation for the geometry corresponding to localized absorption is not yet available, but this geometry is encountered frequently in the analysis of actual samples. Hence, experimental results for model systems, such as the data presented here, are of considerable practical value in the interpretation of photoacoustic measurements.

In this section we discuss the detection and spatial characterization, using a photoacoustic technique, of limited area NaF surface absorption regions deposited on KCl crystals.[27] The size of the surface absorber can be deduced from the photoacoustic signal distribution, as shown in our results. Furthermore, the photoacoustic signal dependence on the laser chopping frequency f was found to be the same as that predicted for thin films in existing one-dimensional models[2,3,4] at both the center and at the boundary of the limited area films. The failure of high power laser window materials such as KCl often results from excessive heating at an inclusion or other defect having higher absorptance than the window itself.[17] Thus, the detection of such absorbers non-destructively is important for the evaluation of high power laser window materials, and photoacoustic spectroscopy has proved to be very useful for this purpose.

Current one-dimensional theoretical models predict that essentially transparent materials having only a surface absorptance will have photo-

acoustic signals inversely proportional to the laser chopping frequency f, and that such materials having only a bulk absorptance will have signals proportional to $f^{-3/2}$. For a surface absorber the thickness of the absorbing layer on the sample is smaller than the thermal diffusion length L_{th}, which is defined by:

$$L_{th} = \left(\frac{D}{\pi f}\right)^{\frac{1}{2}}$$

where D is the thermal diffusivity of the sample.

The experimental apparatus used here is very similar to one previously reported.[11] Briefly, the photoacoustic cell consists of one pure KCℓ window and a second KCℓ window having a defect or absorber. A CO_2 laser operating at 10.6 μm is chopped and then focused by a lens, for the present experiment to a beam size of about 2 mm. The beam passes through the photoacoustic cell and into a power meter. Light absorbed by the sample is converted to heat by non-radiative processes, and the gas in the enclosed cell is periodically heated by conduction from the sample. A pressure fluctuation is produced and detected by the microphone as the photoacoustic signal. A lock-in amplifier is used to detect the root-mean-square value of the fundamental component of the signal. In addition, the photoacoustic cell is mounted on a translation stage which can be moved precisely by a micrometer, and the laser source can scan horizontally across the sample by moving the translation stage. A block diagram of the apparatus is given in Figure 17.

The samples used in this investigation consisted of limited area NaF films of about 3 μm thickness deposited on KCℓ crystals. The film regions were deposited as a circle of 4.1 mm diameter or as a stripe of 4.1 mm width, where the lateral dimensions were measured directly with a traveling microscope for comparison with the photoacoustic measurements as described below. The samples were installed as exit windows of the photoacoustic

cell, with the films facing inside the sealed cell. These samples, consisting of absorbing films on transparent substrates, serve to model transparent crystals having localized, absorbing surface defects.

The photoacoustic signal as a function of beam position, while scanning along a diameter of the circular film regions is shown in Figure 18. Due to the circular profile of the laser beam and the film, and to the intensity distribution in the beam, it was calculated that the 45 signal strength points are associated with the diameter of the film. The diameter was determined photoacoustically to be 4.1 mm in agreement with the results obtained with the traveling microscope. Similar agreement has been obtained for the other sample having an absorbing film stripe. Also shown in Figure 18 is a theoretical signal distribution based on a Gaussian beam profile with a $1/e^2$ intensity radius of 1.08 mm, a radius derived from transmission measurements through apertures.

The chopping frequency response has been measured at two positions, labeled as A and B in Figure 18. In position A the beam was at the center of the circular film, and in position B the beam was at the boundary, or rim, of the circular film. The chopping frequency data are shown in Figure 19. The frequency dependence of the signal at both positions is found to be f^{-1}, as expected for surface absorption. The difference of the signal levels on these two positions is due to the different fractional areas of the film which are illuminated by the laser beam for the center and boundary cases, as was determined by calculation for the beam and sample geometries of this experiment.

In conclusion, photoacoustic measurements have been performed on samples fabricated as absorbing, limited-area NaF films on transparent KCℓ substrates and having surface absorption regions with dimensions of

the same order of magnitude as the incident light beam diameter. Photoacoustic signal data were obtained as a function of beam position to characterize the lateral extent of the absorber at the sample-gas interface. Additionally, photoacoustic signals were obtained as a function of chopping frequency at the center and at the boundary of the films. The functional dependence on the chopping frequency, which is in general associated with the depth distribution of the absorbers, was found to be proportional to f^{-1}, and thus was the same as the functional dependence of theoretical and experimental results for one-dimensional heat flow systems.

An extension of these studies has involved modeling the more general case of a small absorbing inclusion located inside a transparent sample, where the size of the inclusion and its distance from the surface are approximately equal to the thermal diffusion length. These electrical analog samples employed small, tin oxide resistors produced by microtechnology methods and effectively embedded in glass at a known distance from the surface through the use of etched cover glasses of different thicknesses. This procedure, shown schematically in Figure 20 yielded results which were interpretable using one-dimensional heat flow theory, even though the heat flow was three-dimensional by the construction of the samples. These results, shown in Figures 21 and 22, together with a 1-d calibration of the apparatus using planar resistor heat sources, establish the absolute calibration for localized absorption, validates the use of focused beams to reach high intensity levels needed in some semiconductor experiments, and permits the interpretation of data showing more complex features than the normally discussed f^{-1} or $f^{-3/2}$ dependences, where f is the chopping frequency. For the case in which the absorption is localized to a plane at a distance L from the surface, the photoacoustic signal is found to be proportional to $f^{-1} \exp(-L/L_{th})$, where L_{th} is the thermal diffusion length.

Additional effects would be expected to occur for cases in which high temperatures were reached in the vicinity of localized absorbers, due to the temperature dependence of absorption processes, gas density, and gas thermal conductivity.

Section VI

PHOTOACOUSTIC SPECTROSCOPY OF ADSORBED SURFACE IMPURITIES

1. Introduction

Significant infrared absorption can arise from vapors adsorbed on solid surface during exposure to the atmosphere, during exposure to low-vapor-pressure laser system components, and during surface passivation or stabilization treatments. The photoacoustic effect has proved to be a useful quantitative technique for the measurement of surface optical absorption and, when using a CO_2 laser source, provides a sensitivity of a few percent of one monolayer for vapor molecules chemisorbed on highly transparent substrates.

The work described in this section involves an application of photoacoustic spectroscopy to surface absorption studies of high power laser window materials.[28] Results are presented for the time dependence of surface absorption during controlled vapor exposure and for the wavelength dependence of surface absorption, in the 9-11 μm range, following atmospheric contamination. The application of these techniques to the determination of adsorption rate constants, activation energies, and the chemical identification of surface impurities is discussed.

The photoacoustic technique, when using gas coupling between the sample and the microphone, is relatively more sensitive to surface absorption than to bulk absorption due to the lack of attenuation of thermal waves during the heat transport through the solid[8] as was discussed in Section II. An early application of photoacoustic spectroscopy to surface analysis was reported by Rosencwaig.[29] The procedure involved the use of a conventional lamp source and monochromator to

to obtain spectra of highly polished copper electrodes passivated with benzotriazole. Sensitivity with this type of apparatus is better than 1 monolayer at the surface. Since the photoacoustic signal is directly related to the amount of heat produced, improvement in sensitivity can be obtained by increasing the power of the source from the few milliwatts available from the lamp source to the much higher powers available from tunable laser sources. A laser-excited photoacoustic apparatus can detect fractional surface absorption at levels of 10^{-6} and below, while a monolayer of a surface absorber yields a fractional absorption on the order of 10^{-4}. The results discussed here for infrared absorption at the surfaces of highly transparent substrates used fixed-wavelength and tunable CO_2 laser sources operated at lower levels of a few watts in the 9-11 μm wavelength range.

2. Experiment

A block diagram of the apparatus is shown in Figure 23. The CO_2 laser used in the fixed wavelength measurement of the time dependence of the photoacoustic signal during a controlled vapor exposure is an Apollo Laser, Inc. Model 500 operating at 10.6 μm with a maximum output of 50 W cw. This fixed wavelength laser has been modified by replacement of the extraction mirror with a specially coated mirror to avoid the possiblity of oscillation near 9.6 μm. The CO_2 laser used in wavelength dependence studies is an Advanced Kinetics, Inc. Model MIRL-50-SL operating in range of 9.2 to 10.9 μm with a maximum output of 35 W cw averaged over all lines. This turnable laser is equipped with a Sargent-Welch Model 8821 mechnical pump for high gas throughput in order to reach higher cw power levels. The power meter is a Coherent Radiation, Inc. Model 201. The condenser microphone is a Brüel and Kjaer Model 4134

followed by a Model 2619 preamplifier. The lock-in amplifier is a Princeton Applied Research Corp. Model 129A modified to accept a Model 189 selective amplifier stage.

The aluminum photoacoustic cell has a cavity of approximately 0.5 cm thickness and 1.3 cm diameter. The cavity is enclosed by two samples (laser windows) clamped against gaskets. The acoustic signal in the cell is coupled to the microphone through a 13-gauge hypodermic needle. The cell has valves which permit purging or filling with gases other than air when necessary. The absolute absorption calibration of the photoacoustic cell was accomplished by use of an electrically heated thin film resistor mounted on the cell, to which a known electrical power was supplied, and for which the acoustic response was measured.[11] The wavelength calibration of the tunable laser was obtained using an Optical Engineering, Inc. Model 16-A spectrum analyzer, for which the calibration was verified using a HeNe laser. The photoacoustic cell was operated with a slight rotation away from normal incidence to bring reflections away from the laser cavity and to eliminate some possible interference effects.[11] The chopping frequency for the data presented here was 33 Hz.

The controlled vapor source consists of a three-stage gas dispersion apparatus constructed from 500 ml Erlenmeyer flasks having medium and coarse porosity gas dispersion tubes submerged in the first and second stages, respectively, and a straight glass tube submerged in the final stage. Ultra-pure nitrogen carrier gas was passed through each of the partially filled flasks, which contained saturated solutions of NaCl in deionized water, with approximately a 20% excess of NaCl. The flow rate was typically set at a few cubic centimeters per minute to provide a constant replacement of gas in the cell from the constant relative humidity source above the saturated solutions. The technique is related to that recently reported

for a higher flow rate apparatus.[30]

The polished KCl and NaCl crystals discussed in this report were purchased from the Harshaw Chemical Company, Part Number L-02505, and further selected for low total absorption.

3. Results

An example of results obtained for the time dependence of the photoacoustic signal during a controlled vapor exposure following a chemical etch is given in Figure 24. The etching procedure is a standard one consisting of two minutes in HCl followed by 10 sec rinses in ethanol and two isopropanol rinses followed by drying with a hot air blower. The procedure was to expose the etched KCl crystals to the vapor derived from the saturated NaCl solution continuously, except during the actual photoacoustic measurement, when the valves of the cell were closed. Similar results have been obtained with NaCl crystals. The initial portion of the curve, represented by the dashed line, includes laser beam exposure-time effects, as discussed below, in addition to effects from elapsed-time or vapor exposure-time, as plotted on the horizontal axis.

In general, in experiments involving both KCl and NaCl laser windows, effects were observed which were separately associated with desorption of contaminants (having a beam exposure-time dependence) gas desorption (having a vapor exposure-time dependence) and local heating (having a laser power-level dependence). The choice of only a few watts for the laser output power in the experiments reported here was to eliminate any significant contribution from the latter effect above, which can be important at higher power levels on crystals having localized, highly absorbing defects which can produce temperature dependent absorption.

Some initial results for the wavelength dependence of the photoacoustic signal during a controlled vapor exposure is given in Figures 25(a) through 25(c). These data are for KCl crystals (a) 1 day after etching and mounting in cells filled with ultra-pure nitrogen, (b) after 4 days exposure to vapor derived from the saturated NaCl solution in deionized water, and (c) the difference spectrum for data obtained after and before vapor exposure.

Finally, in Figure 26 results are shown for the wavelength dependence of the photoacoustic signal for a pair of etched crystals, which were first stored mounted in the cell filled with ultra-pure nitrogen for 1 day, then exposed to atmospheric contamination for 7 days by storing in a glass cover dish with dessicant. The contribution to the signal shown in Figure 26 from the background signal (existing prior to atmospheric exposure) is approximately 12% of the total signal.

4. Discussion

The contributions to the total photoacoustic signal, as shown in Figure 24, and as inferred from that data and from additional measurements on NaCl and KCl crystals, can be viewed as (1) a background signal arising from bulk and surface impurities and defects, (2) a "first layer" fast-rate surface adsorption which occurs during, and just after, etching, and (3) a "second-layer" slow-rate adsorption process occurring during the vapor exposure. These processes are shown schematically in Figure 27. The latter process is the time dependent portion of the signal represented by the solid line in the Figure 24. The consideration of the surface adsorption effects as two processes has been put forth previously by Bennett during a discussion of water contamination of thin films in connection with the work of Sparks.[31]

The data of Figure 25 show general trends for adsorption after etching consistent with that observed previously by other workers.[32] The difference spectrum in 25(c) demonstrates the capability of this technique to provide chemical identification of adsorbates. The tentative association, by the design of the experiment, which involved the water vapor exposure of a hygroscopic substrate, is with adsorbed water. This identification is, of course, subject to further measurements and calculations. Internal molecular vibration modes for water would not correspond to peaks in the 9-11 μm range, but quite possibly vibrations of the molecule associated with the (weaker) chemisorption bonds would. The character of the etched surface, the adsorption site heterogeneity, and the various possible adsorption orientations combine to make this a relatively complex problem, however.

The data of Figure 26 are primarily of interest for the demonstration of the relatively large surface absorption change that occurs with atmospheric contamination and also its relatively broad wavelength dependence. The application of this type of measurement (which employs uncontrolled exposure conditions) would be primarily in the testing or handling of assembly environments for laser or optical systems.

For a precisely characterized substrate and adsorbing-molecule system, the analysis of data such as that shown in Figure 24 will yield an effective rate constant for the adsorption process (or the actual rate constant for a less heterogeneous system). Extension to the analysis of the temperature dependence for such a system would yield the effective activation energy of the process and, in turn, provide information on useful operating or exposure parameters for optical systems.

For the purpose of comparison with other work, it should be noted

that the conversion from photoacoustic signal expressed as μV/watt (root-mean-square photoacoustic signal per average optical power transmitted) to the fractional absorption per surface for pure surface absorption or for surface absorption changes for KCl windows is made by multiplying by a factor of 2.0×10^{-5}. This yields, for example, a change in surface absorptance in the difference spectrum of Figure 25 amounting to 3.0×10^{-4} at a wavelength of 10.6 μm.

5. Conclusion

A photoacoustic technique has been applied to the study of adsorbed surface impurities on alkali halide materials of interest in high power laser systems. The sensitivity of the method corresponds to a few percent of a single monolayer for a chemisorbed species such as water vapor. The technique could be extended, with the addition of ultra-high vacuum processing techniques, precisely characterized substrate crystals, and detailed monitoring of exposure-gas composition, to provide fundamental information on particular substrate-adsorbate systems. However, many practical applications in the development of high power laser systems, such as the investigation of surface absorption due to vapors adsorbed on laser window surfaces during exposure to the atmosphere, during exposure to low-vapor-pressure system components, and during surface passivation treatments, correspond to less stringent experimental conditions such as those used for the initial investigations described here. To improve the operation of the spectrometer and to permit easier tuning and more rapid data collection, a precision ratiometer has been designed and constructed to allow monitoring of the photoacoustic-signal to transmitted-power ratio during tuning of the laser. Additionally, the system enclosure was modified to permit continuous monitoring of the

wavelength calibration when needed.

An additional capability of the spectrometer is indicated by the curve shown in Figure 28. This diagram represents a portion of an absorption spectrum for an adsorbed gas layer on a solid surface. Normally, the absorption level is obtained at several CO_2 laser line positions (represented in the figure by vertical solid lines, with there being at least 80 useful lines available from the tunable laser). In many cases, this information would uniquely identify a small molecule. It would also be possible in some cases to use the piezoelectric frequency scanning capabilities of the laser to scan near a line, if the spectrum shows several absorption features within the tuning range of a single line. This procedure would further contribute to the precise identification of an impurity.[33]

Section VII

VISIBLE WAVELENGTH SPECTROSCOPY OF II-VI SEMICONDUCTORS

In this section experimental and computational results for some visible wavelength studies of II-VI semiconductor crystals are described. In particular, optical and photoacoustic data are compared for measurements on ZnSe and CdS crystals. Additionally, results are given for the effective optical absorption coefficient as derived from the experimental optical transmission data and from the photoacoustic data for the samples.

A block diagram of the experimental apparatus is shown in Figure 29. The light source is a 1 kW xenon lamp with a Schöffel Model Gm-250 monochromator operated with a 2 mm slit-width, giving a 6.6 nm bandpass, and followed by a 390 nm long pass filter to eliminate second and higher order diffracted light. The chopper is a Laser Precision Model CTX 534 which was normally operated at 10 Hz. The condenser microphone is a Brüel and Kjaer Model 4134 followed by a Model 2619 preamplifier giving an overall sensitivity of 1 mV/μbar. The lock-in is a Princeton Applied Research Corporation Model HR-8, which has a tuned amplifier stage and detects the root-mean-square value of the fundamental component of the photoacoustic signal. The visible wavelength photoacoustic cell has a cavity of 15 mm in diameter and a length of 8 mm, including 1 mm due to the thickness of the gasket. The cell has been previously described by Campbell et al.[34]

The samples were approximately square with a size of about 5 mm and thicknesses of 0.41 mm for ZnSe and 0.35 mm for CdS. For each semiconductor sample, a reference sample was cut from the adjacent portion of the same

crystal and coated on its front side with flat-back paint. This reference sample was used to normalize the photoacoustic signal and to correct for the spectrum of the source. All crystals were mounted on square sections of glass microscope slides using a cyanoacrylate ester glue, and these glass slide sections were the exit window of the photoacoustic cell as shown in Figure 29.

The normalized photoacoustic spectra of ZnSe and CdS are shown in Figures 30 and 31, respectively. The photoacoustic spectra show absorption edges at 469 nm for ZnSe and 520 nm for CdS. The absorption edge is defined here as the point near the band edge where the slope is a maximum. The spectrophotometer data are given in Figures 32 and 33 for ZnSe and CdS, respectively. These data were obtained with a Varian Superscan 3 visible spectrometer using a resolution of 1 nm. The optical spectra show absorption edges at 473 nm for ZnSe and 520 nm for CdS.

A computer program based on a multilayer one-dimensional heat-flow model of the photoacoustic cell was used to calculate the signal magnitude as a function of the absorption coefficient of the semiconductor crystals. This procedure permits a comparison of data from a photoacoustic spectrum with the optical spectrum for the same crystal. The calculated data shown in Figures 34 and 35 include necessary reflectivity results derived from published data[35,36] and include an adjustment to the magnitude of the calculated photoacoustic data to match the value of the maximum absorption coefficient of the calculated optical data. The absorption edges occur at 471 nm for ZnSe and at 523 nm for CdS in the calculated photoacoustic spectra and at 473 nm for ZnSe and 522 nm for CdS in the calculated optical spectra. Note that the effect of the heat-flow-model data-conversion, as illustrated in the results for the transformed data presented in Figures

34 and 35 is to bring the photoacoustic data into closer conformity to the the results derived from conventional optical transmission spectrometer measurements.

Section VIII

SUMMARY

A list of topics investigated during the course of this work is given below to summarize the general scope of this project:

1) Theoretical calculations for a one-dimensional heat transport and acoustic wave propagation model for the photoacoustic cell were performed. The results obtained demonstrate effects of sample thickness, cell length, chopping frequency, and absorption coefficient.

2) An electrical calibration procedure was developed using thin-film resistors or bulk resistor samples, as appropriate. The measured signal level for a known power input to a resistor gives the absolute calibration and frequency response for the cell.

3) An experimental apparatus was designed and constructred for use with CO_2 lasers. The facility presently includes a fixed wavelength laser operating at 10.6 μm and a tunable laser operating between 9.2 and 10.9 μm.

4) Optical absorption determinations for high power laser windows were performed. There included RbCl-doped KCl laser windows provided by the Air Force Materials Laboratory which had been separately characterized by laser calorimetry.

5) Procedures were devleoped for the assessment of the deterioration and surface treatment of high power laser window materials and transparent materials in general.

6) Optical absorptance measurements were performed for window coating materials, including contaminated NaF films for which transmission infrared spectrophotometer scans were also obtained.

7) The application of the photoacoustic technique to the detection and characterization of localized defects has been investigated. This included the procedures of beam scanning and derivation of the depth distribution of absorption coefficient from the chopping response data.

8) The measurement of nonlinear absorption effects using photoacoustic detection has been demonstrated, initially using GaAs:Cr and Si samples.

9) An apparatus using a 1 kW xenon lamp source with monochromator (which was originally constructed in connection with biological materials research) has been adapted for and applied to the analysis of semiconductors and contaminated film.

10) Controlled vapor exposure studies of transparent crystal surfaces have been performed using the fixed wavelength CO_2 laser. These studies have revealed several new general features which are separately associated with the desorption of contaminants (having a beam exposure-time dependence) and gas adsorption (having a vapor exposure-time dependence).

11) The absorption bands due to impurities in highly transparent materials and due to gases adsorbed on their surfaces have been investigated in the 9.2 to 10.9 μm wavelength range.

12) Visible wavelength photoacoustic and optical measurements have been performed on II-VI semiconductor crystals and effective optical absorption coefficients have been derived from the data using, for the photoacoustic results, a multilayer one-dimensional heat-flow model of the cell.

Section IX

REFERENCES

1. A. G. Bell, Am. J. Sci. 120, 305 (1880).
2. J. G. Parker, Appl. Opt. 12, 2974 (1973).
3. A. Rosencwaig and A. Gersho, J. Appl. Phys. 47, 64 (1976).
4. H. S. Bennett and R. A. Forman, J. Appl. Phys. 48, 1432 (1977).
5. L. C. Aamodt and J. C. Murphy, J. Appl. Phys. 49, 3036, (1978).
6. A Hordvik and L. Skonik, Appl. Opt. 16, 2919 (1977).
7. A Rosencwaig, J. Appl. Phys. 49, 2905 (1978).
8. J. F. McClelland and R. N. Kniseley, Appl. Phys. Lett. 28, 467 (1976).
9. K. L. Lee, M.S.E.E. Thesis, University of Washington, 1978.
10. M. A. Afromowitz, K. L. Lee, and S. S. Yee, in Proceedings of the High Power Laser Optical Components and Component Materials Meeting, 1977, p. 219.
11. J. M. McDavid, K. L. Lee, S. S. Yee, and M. A. Afromowitz, J. Appl. Phys. 49, 6112 (1978).
12. M. A. Afromowitz, P. S. Yeh, and S. S. Yee, J. Appl. Phys. 48, 209 (1977).
13. G. C. Wetsel, Jr. and F. A. McDonald, Appl. Phys. Lett. 30, 252 (1977).
14. F. A. McDonald and G. C. Wetsel, Jr., J. Appl. Phys. 49, 2313 (1978).
15. M. D. Crisp, N. L. Boling, and G. Dube, Appl. Phys. Lett. 21, 364 (1972).
16. R. Weil, J. Appl. Phys. 40, 2857 (1969).
17. M. Sparks and C. J. Duthler, J. Appl. Phys. 44, 3038 (1973).
18. E. L. Kerr, Appl. Opt. 12, 2520 (1973).
19. M. J. Soileau et al., in Laser Induced Damage in Optical Materials: 1976, NBS Spec. Publ. 462 (U.S. GPO, Washington, D.C., 1976), p. 264.

20. J. R. Fenter, Air Force Materials Laboratory Report #AFML-TM-LP-76-5, (1976).

21. D. L. Stierwalt and M. Hass, in Proc. Fourth Annual Conference on Infrared Laser Window Materials, 1975, p. 7.

22. J. M. McDavid, S. S. Yee, and M. A. Afromowitz, in Technical Digest, Topical Meeting on Photoacoustic Spectroscopy (Optical Society of America, Washington, D.C., 1979), p. ThA8-1.

23. C. C. Ghizoni, M. A. A. Siqueira, H. Vargas, and L. C. M. Miranda, Appl. Phys. Letter 32, 554 (1978).

24. S. K. Gulati and W. W. Grannemann, in Laser Induced Damage in Optical Materials: 1976, NBS Spec. Publ. 462 (U.S. GPO, Washington, D.C., 1976) p. 357.

25. Y. H. Wong, R. L. Thomas and G. F. Hawkins, Appl. Phys. Lett. 32, 538 (1978).

26. H. K. Wickramasinghe, R. C. Bray, V. Jipson, C. F. Quate, and J. R. Salcedo, Appl. Phys. Lett. 33, 923 (1978).

27. T. T. Wang, J. M. McDavid, and S. S. Yee, Appl. Opt. 18, 2354 (1979).

28. J. M. McDavid and S. S. Yee, in Laser Induced Damage in Optical Materials: 1980, NBS Spec. Publ. xxx (U.S. GPO, Washington, D.C., 1981), p. x.

29. A. Rosencwaig, in Optoacoustic Spectroscopy and Detection, Y.-H. Pao, ed. (Academic Press, New York, 1977), p. 193.

30. O. Nakamura, I. Ogino, and T. Kodama, Rev. Sci. Instrum. 50, 1313 (1979).

31. M. Sparks, in Laser Induced Damage in Optical Materials: 1976, NBS Spec. Publ. 462, A. J. Glass and A. H. Guenther, eds. (U.S. GPO, Washington, D.C., 1976), p. 203.

32. J. W. Davisson, M. Hass, P. H. Klein, and M. Krulfeld, in Third Conference on High Power Infrared Laser Window Materials, November 12-14, 1973, Volume I: Optical Properties, C. A. Pitha and B. Bendow, eds., p. 31, (1974).

33. P. C. Claspy, in Optoacoustic Spectroscopy and Detection, Y.-H. Pao, ed. (Academic Press, New York, 1977), p. 133.

34. S. D. Campbell, S. S. Yee, and M. A. Afromowitz, IEEE Trans. Biomedical Eng. BME-26, 220 (1979).

35. J. L. Freeouf, Phys. Rev. B 7, 3810 (1973).

36. M. Cardona, M. Weinstein, and G. A. Wolff, Phys. Rev. 140, A633 (1965).

Figure 1

GEOMETRY OF A CYLINDRICAL PHOTOACOUSTIC CELL

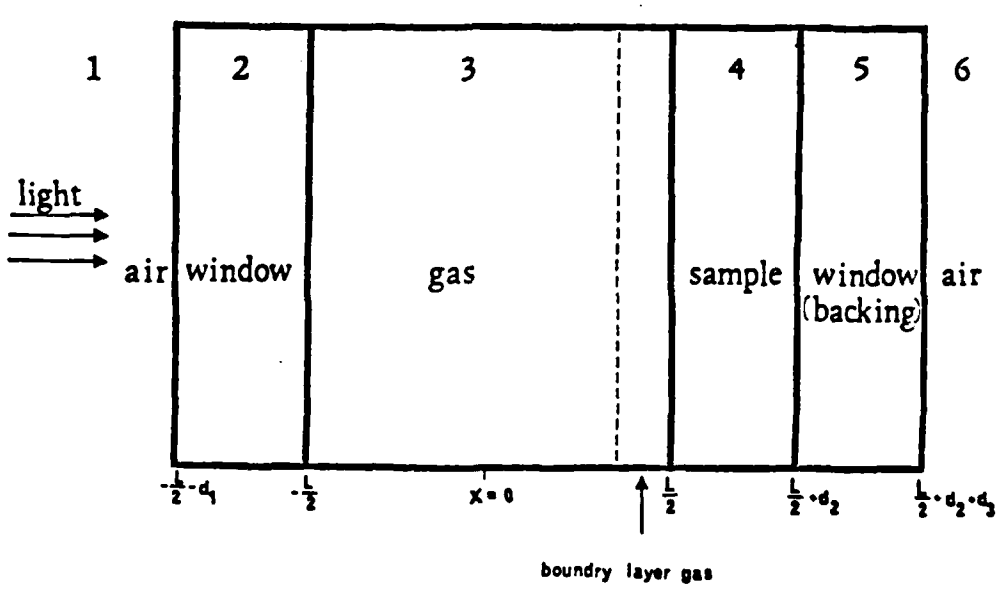

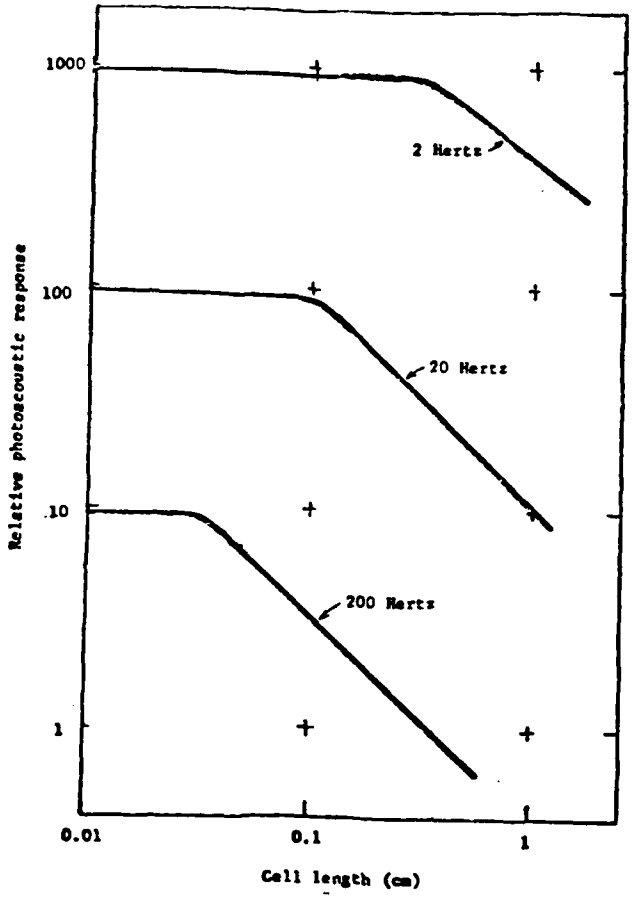

Figure 2

EFFECTS OF CELL LENGTH

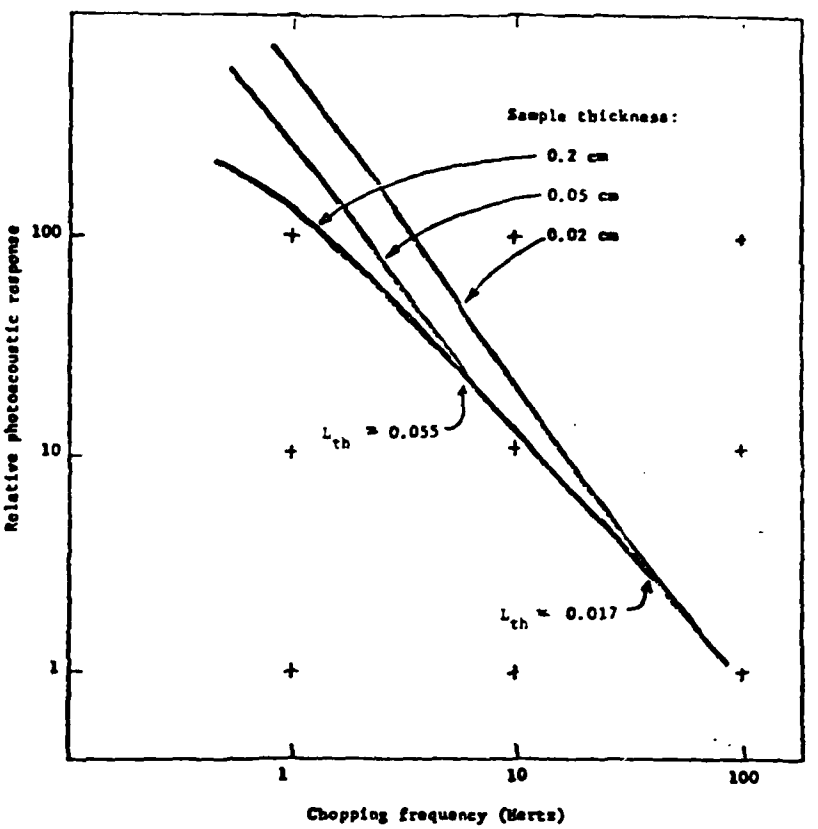

Figure 3

EFFECTS OF SAMPLE THICKNESS

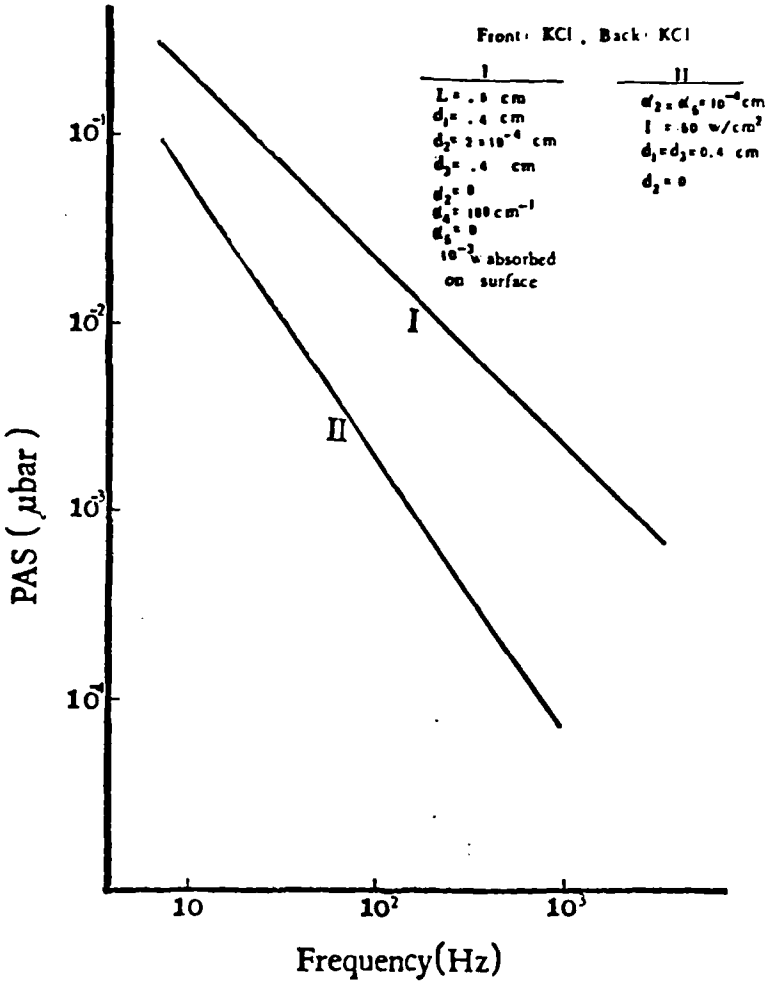

Figure 4

FREQUENCY RESPONSE FOR SURFACE AND BULK ABSORPTION

Figure 5

BLOCK DIAGRAM OF THE PHOTOACOUSTIC APPARATUS
(CHOPPED MODE)

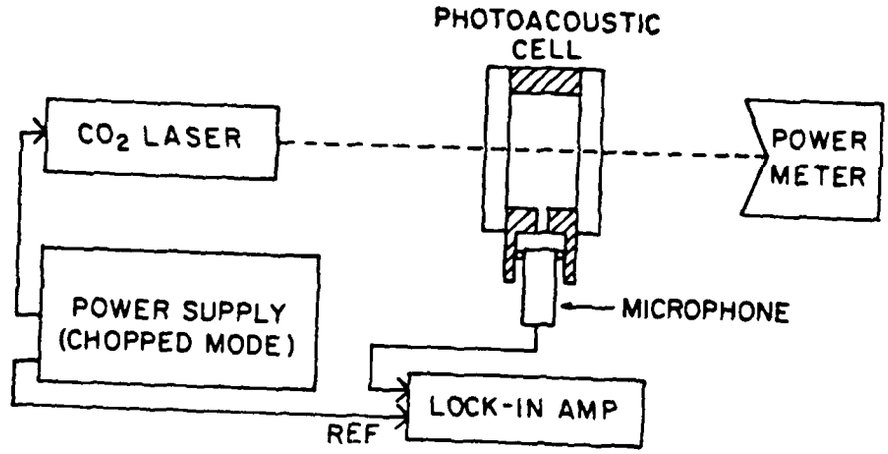

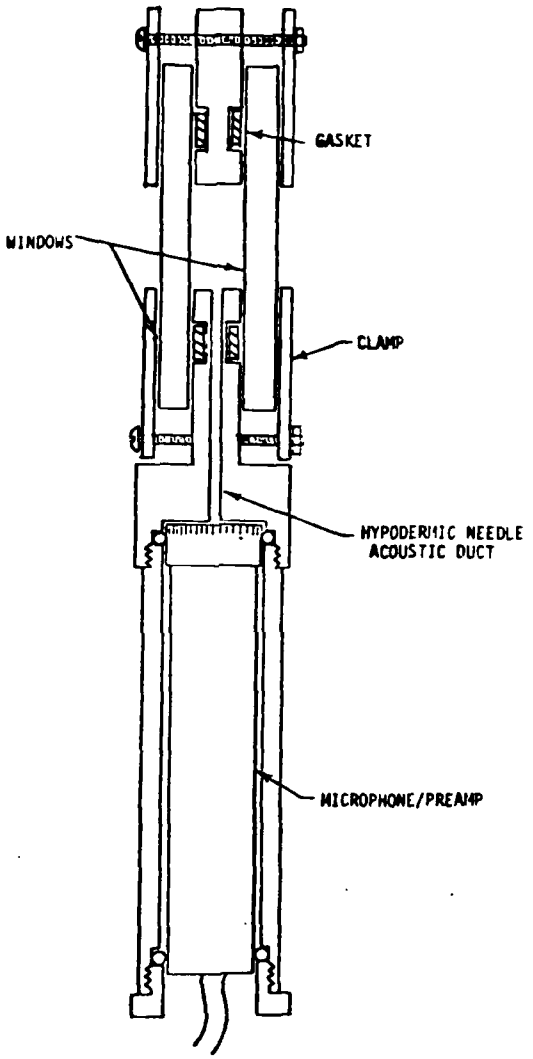

Figure 6

CROSS-SECTION VIEW OF THE PHOTOACOUSTIC
CELL AND THE MICROPHONE/PRE-AMP

Figure 7

ELECTRICAL CALIBRATION PROCEDURE USING A THIN-FILM RESISTOR

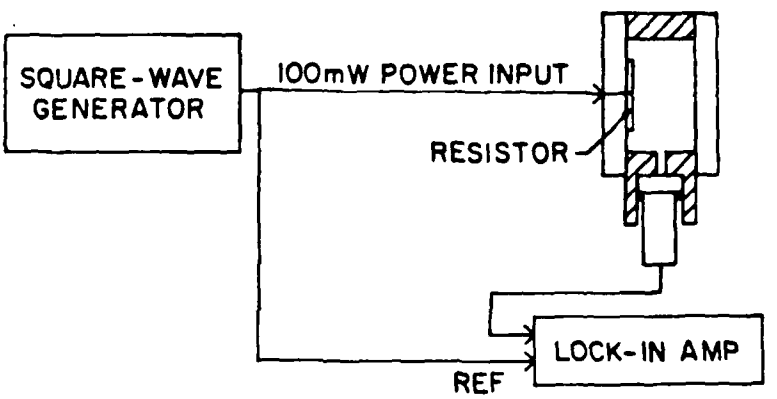

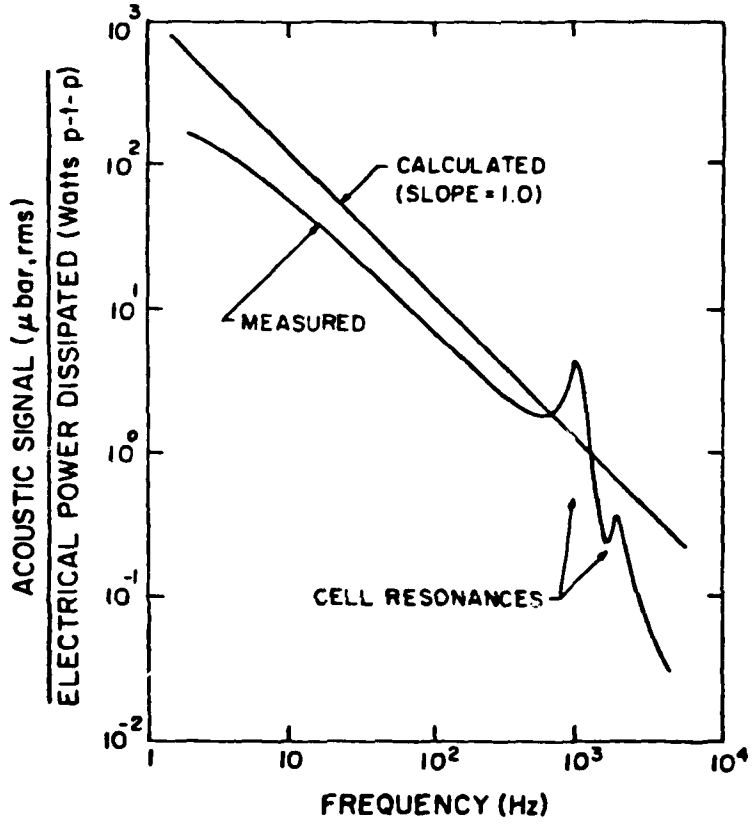

Figure 8

PHOTOACOUSTIC CELL RESPONSE AS MEASURED FOR THE CELL USED AND AS CALCULATED FOR A SIMPLE MODEL.

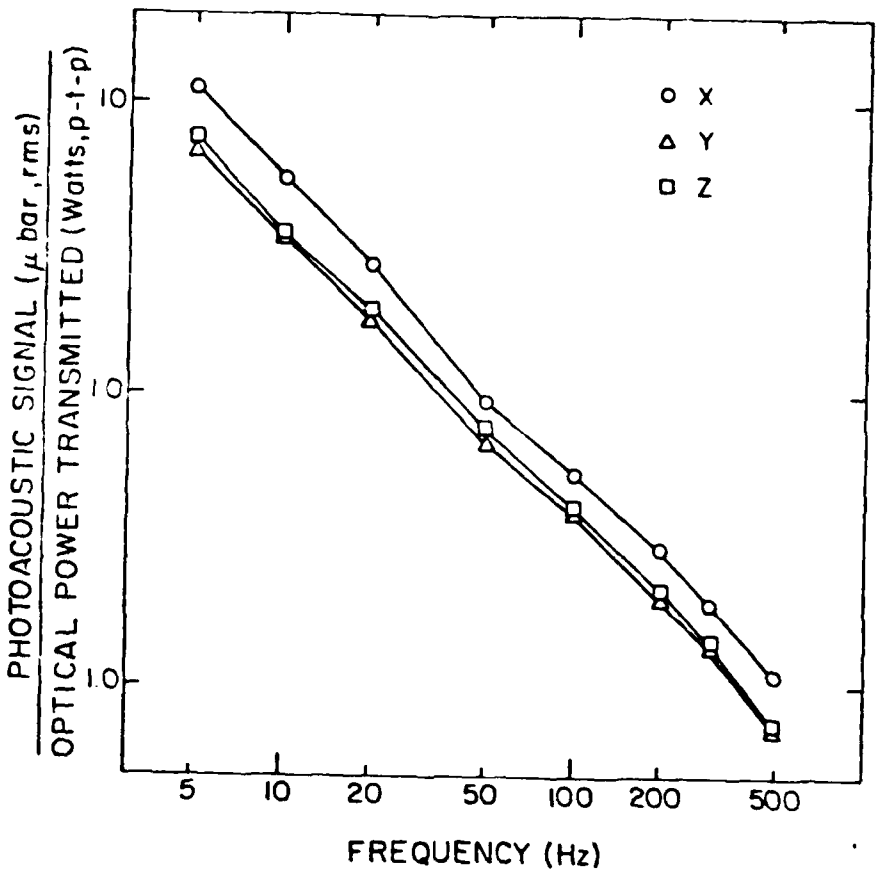

Figure 9

PHOTOACOUSTIC SIGNALS FROM NaF FILMS JUST AFTER REMOVING FROM THE EVAPORATION SYSTEM (SAMPLES Y AND Z) AND AFTER DETERIORATION WITH ATMOSPHERIC EXPOSURE (SAMPLE X).

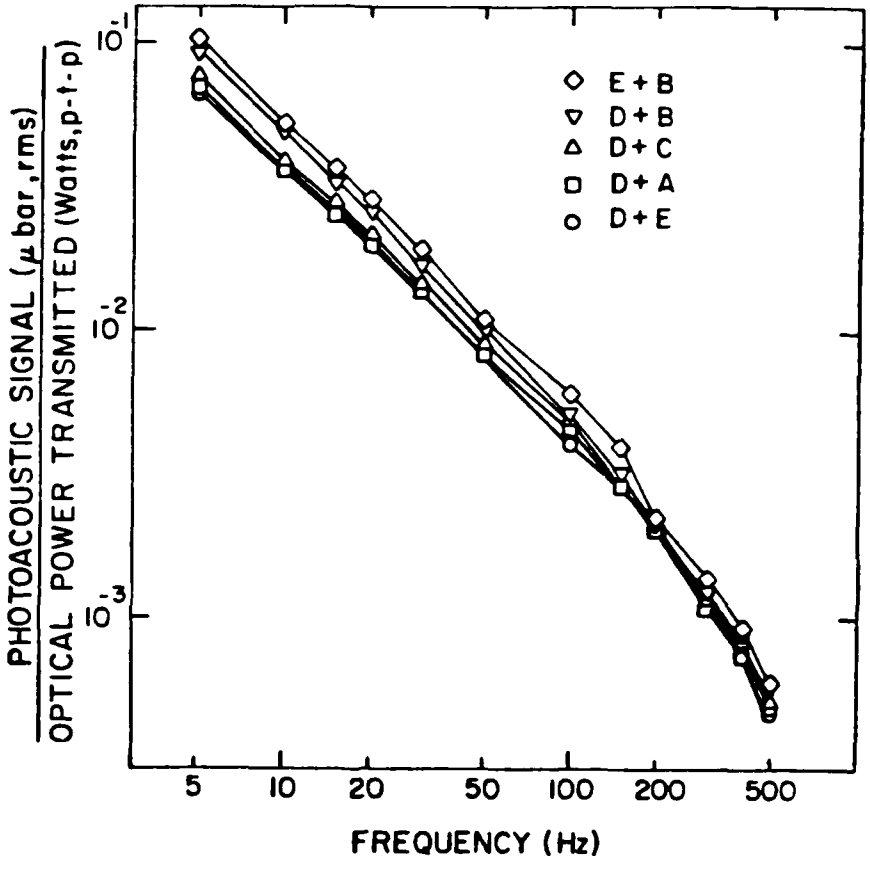

Figure 10

PHOTOACOUSTIC SIGNALS FROM PAIRS OF RbCl-DOPED KCl CRYSTALS

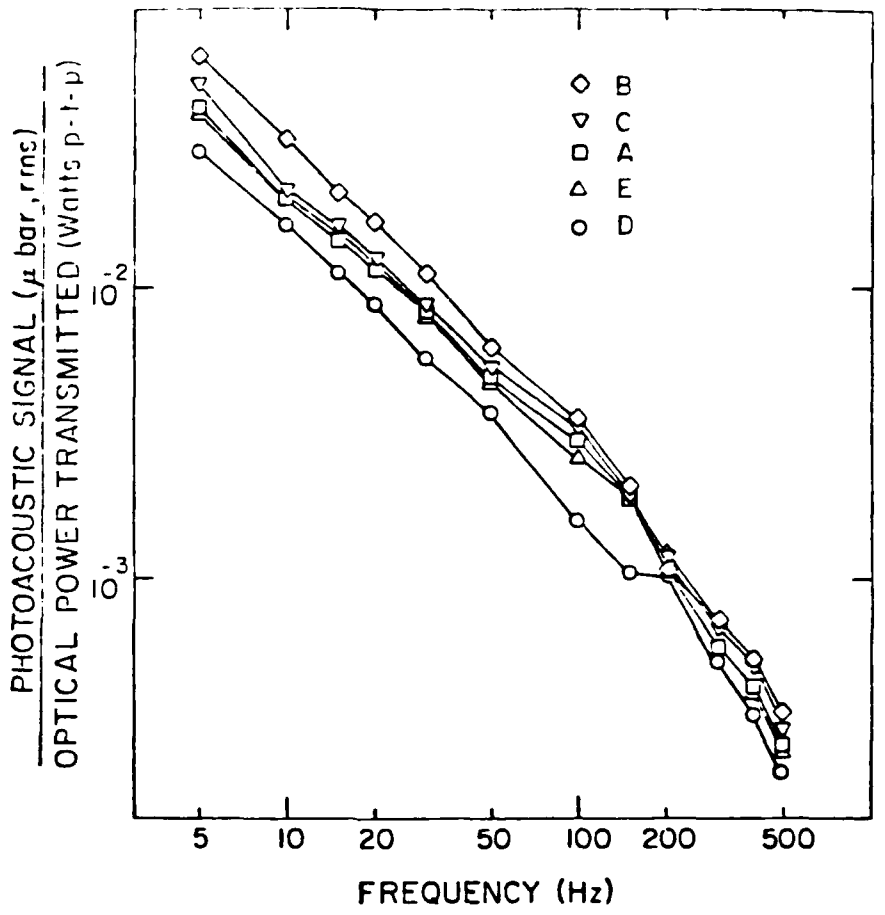

Figure 11

PHOTOACOUSTIC SIGNALS DUE TO INDIVIDUAL RbCl-DOPED KCl CRYSTALS

Figure 12

SIGNAL FLUCTUATION IDENTIFIED WITH INTERFERENCE EFFECTS AND ITS ELIMINATION BY A SMALL ROTATION OF THE CELL. DATA ARE FOR 100 Hz (O) OR ARE SCALED TO 100 Hz USING THE EXPERIMENTAL FREQUENCY DEPENDENCE (Δ).

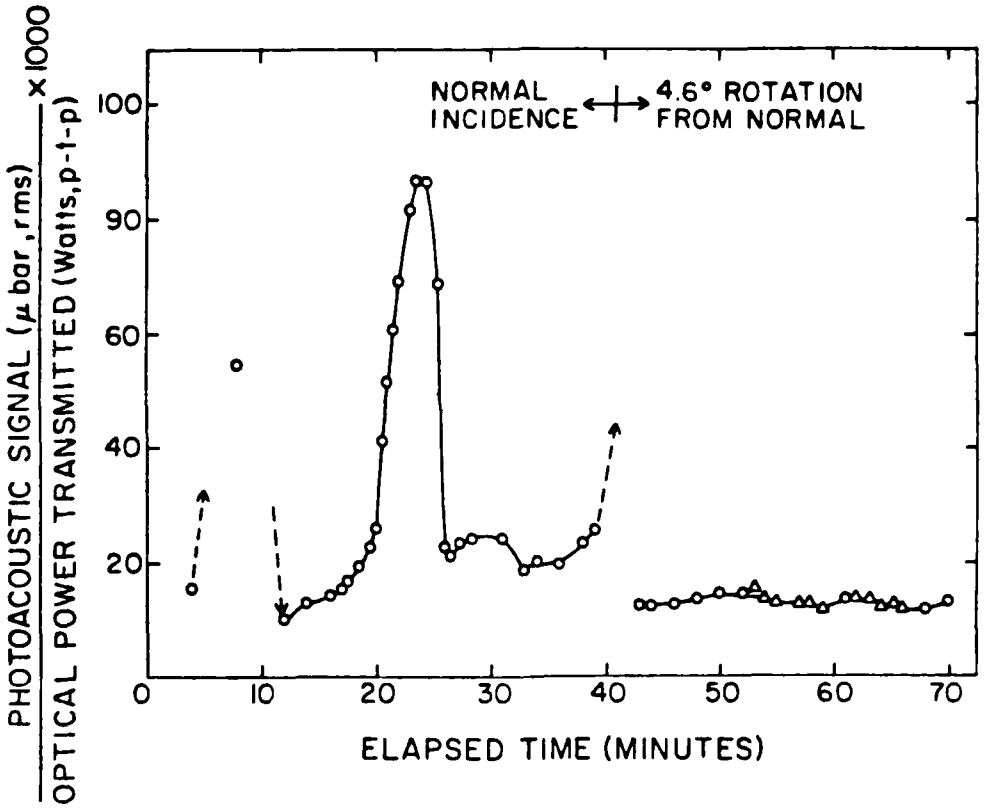

Figure 13

BLOCK DIAGRAM OF THE PHOTOACOUSTIC APPARATUS
(PULSED MODE)

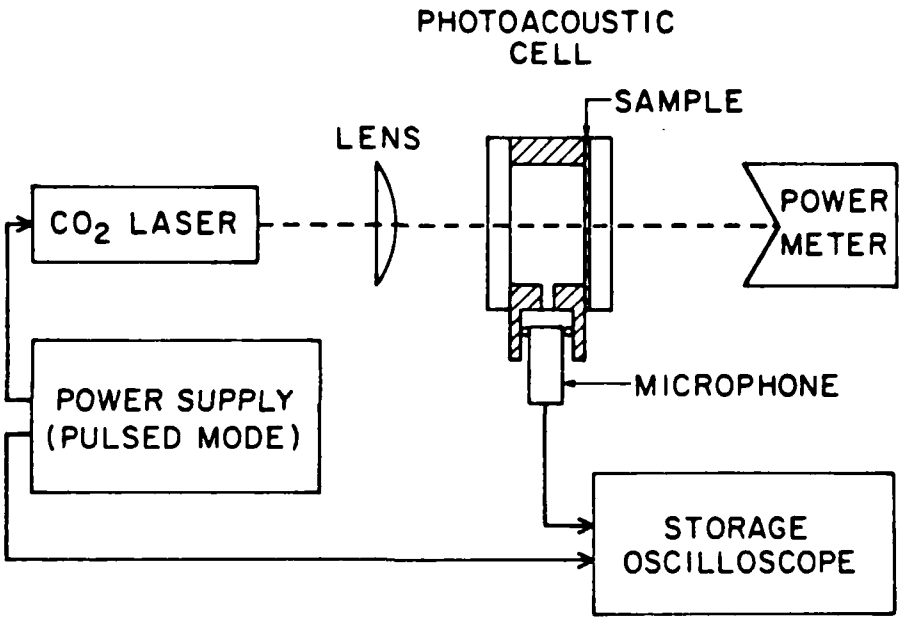

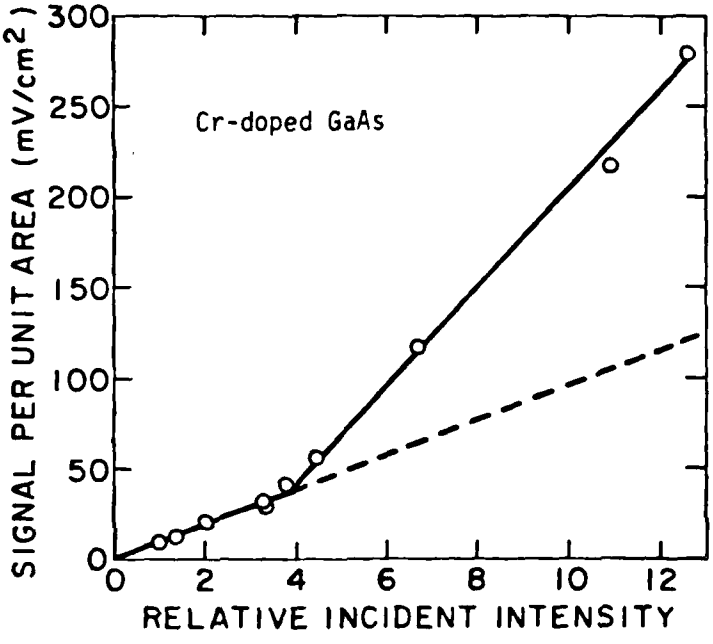

Figure 14

PHOTOACOUSTIC SIGNAL PER UNIT IRRADIATED AREA
VERSUS RELATIVE INCIDENT INTENSITY

Figure 15

PHOTOACOUSTIC RESPONSE TO 0.5 ms PULSES
(FOR BULK AND SURFACE ABSORPTION)

5.0 mm Si

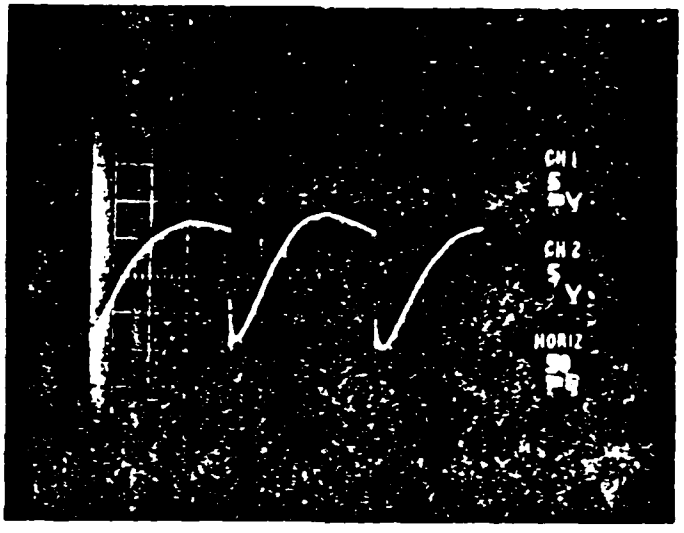

1.7 μm NaF

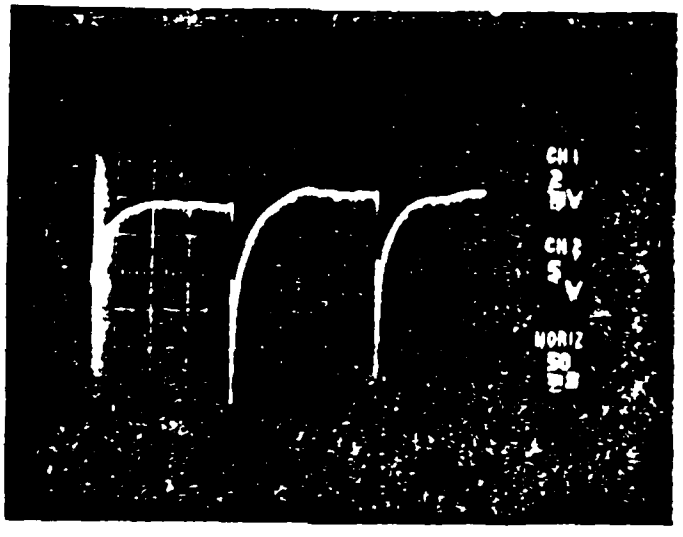

Figure 16

PHOTOACOUSTIC RESPONSE TO 0.5 ms PULSES
(FOR THIN CRYSTALS OF GaAs:Cr AND Si)

15 mil GaAs:Cr

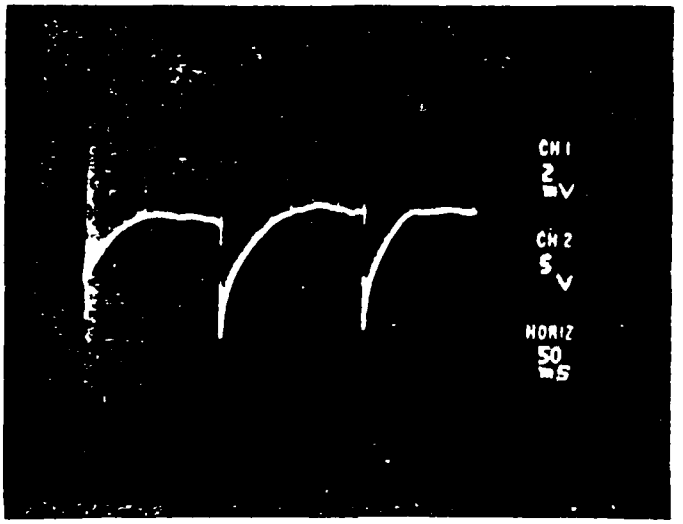

8 mil Si

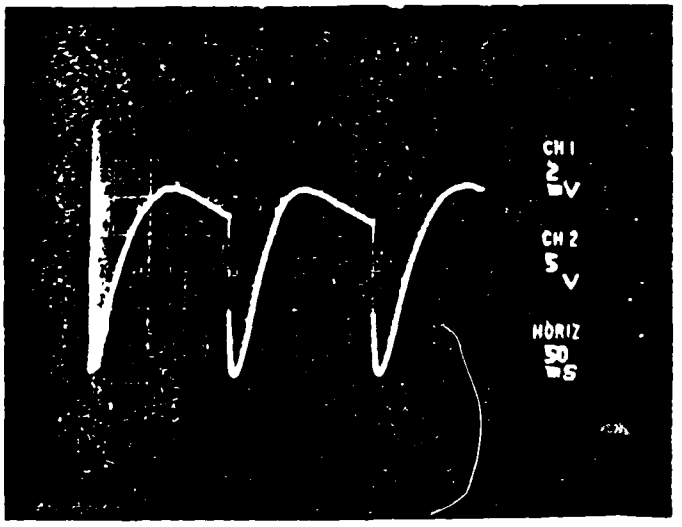

Figure 17

BLOCK DIAGRAM OF THE PHOTOACOUSTIC APPARATUS
(LOCALIZED ABSORPTION)

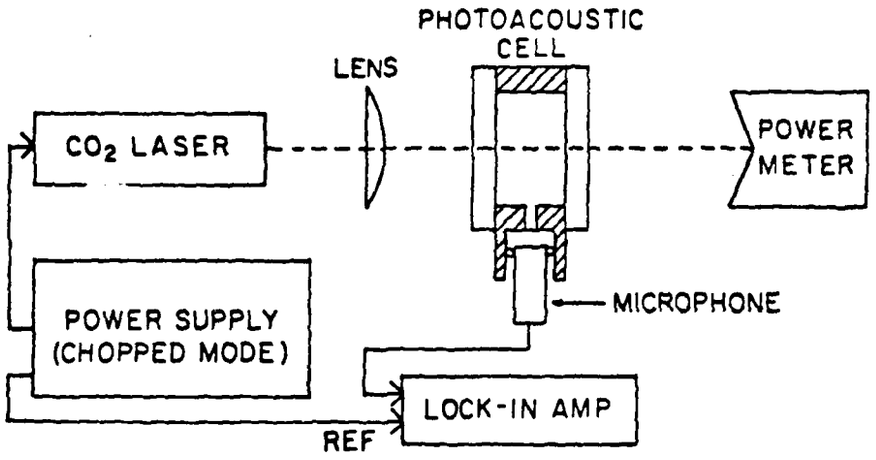

Figure 18

EXPERIMENTAL POSITION DEPENDENCE OF THE PHOTOACOUSTIC SIGNAL (SOLID CURVE) AND CALCULATED DEPENDENCE FOR A GAUSSIAN BEAM (DASHED CURVE)

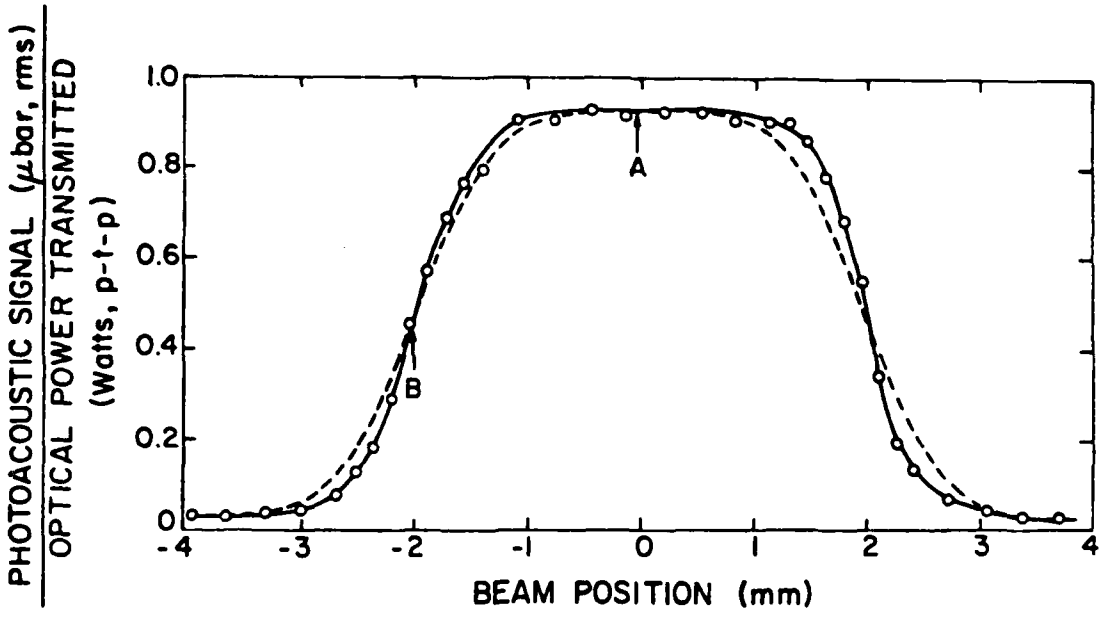

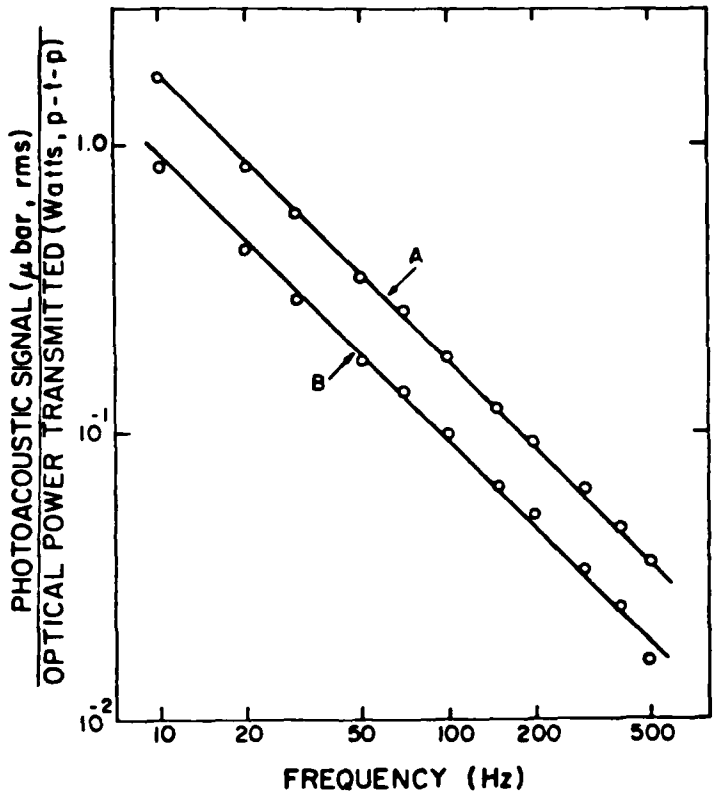

Figure 19

CHOPPING FREQUENCY DEPENDENCE OF THE PHOTOACOUSTIC SIGNAL AT THE CENTER OF THE CIRCULAR FILM (CURVE A) AND AT ITS BOUNDARY (CURVE B).

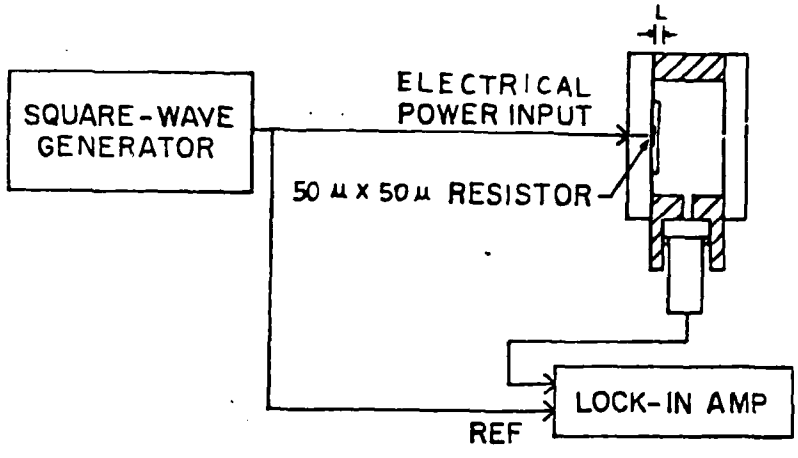

Figure 20

EXPERIMENT CONFIGURATION FOR ELECTRICAL ANALOG OF A LOCALIZED ABSORBER

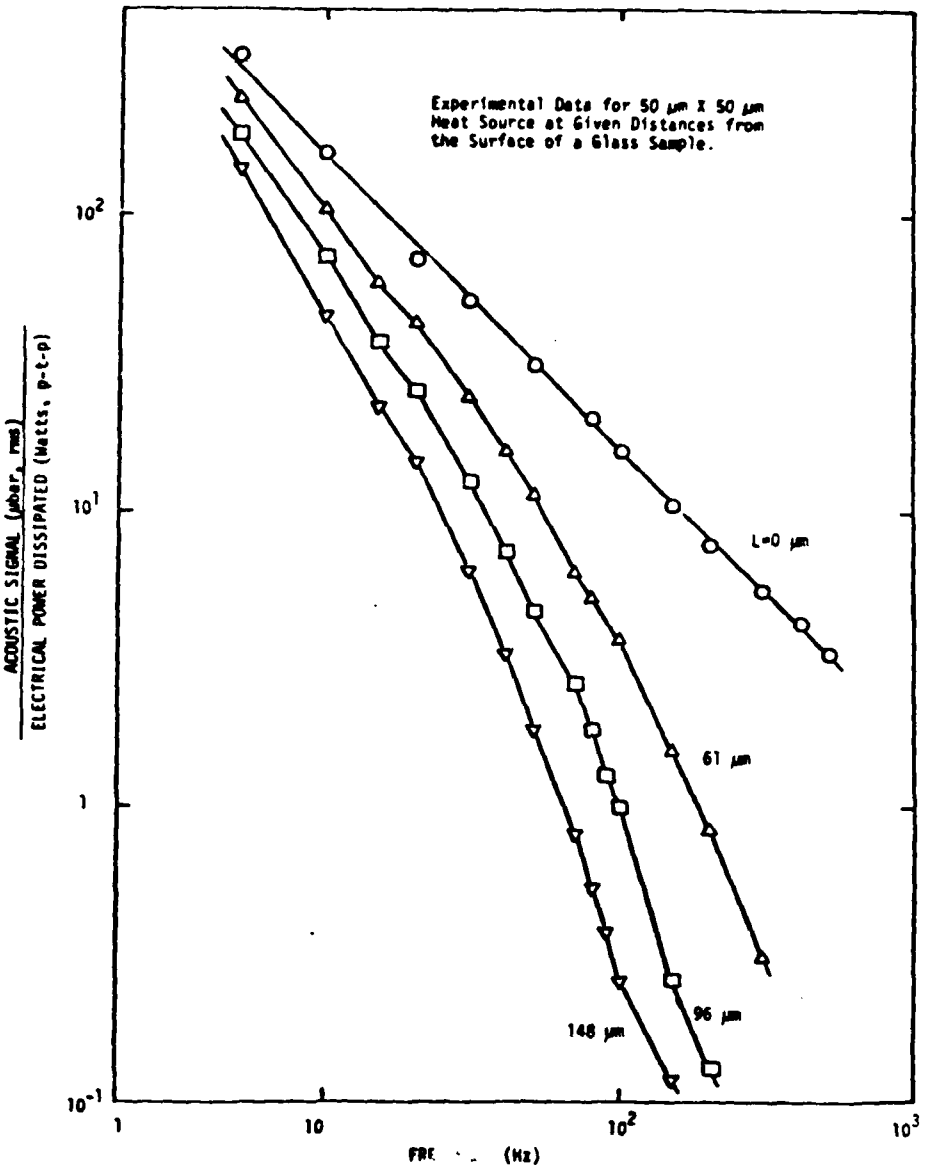

Figure 21

EXPERIMENTAL FREQUENCY RESPONSE FOR 50 μm SQUARE HEAT SOURCE

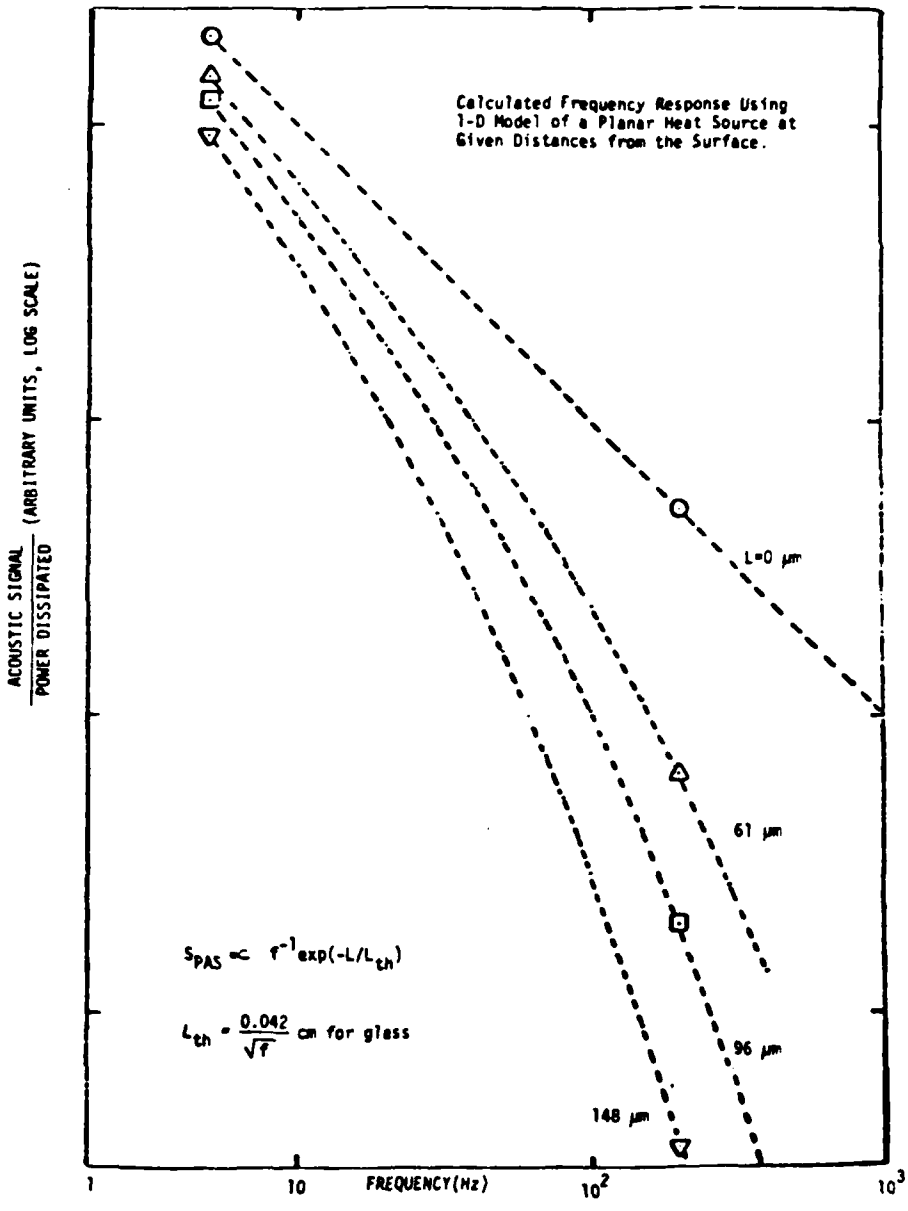

Figure 22

CALCULATED FREQUENCY RESPONSE FOR A PLANAR HEAT SOURCE

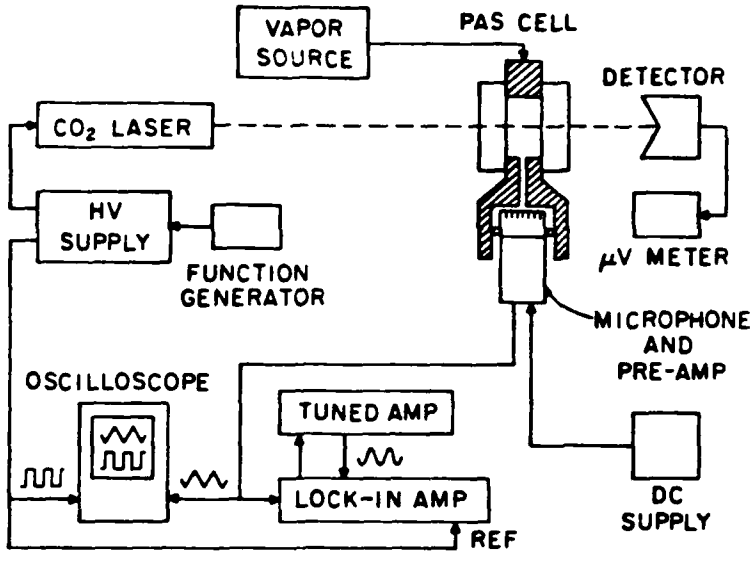

Figure 23

BLOCK DIAGRAM OF THE INFRARED APPARATUS

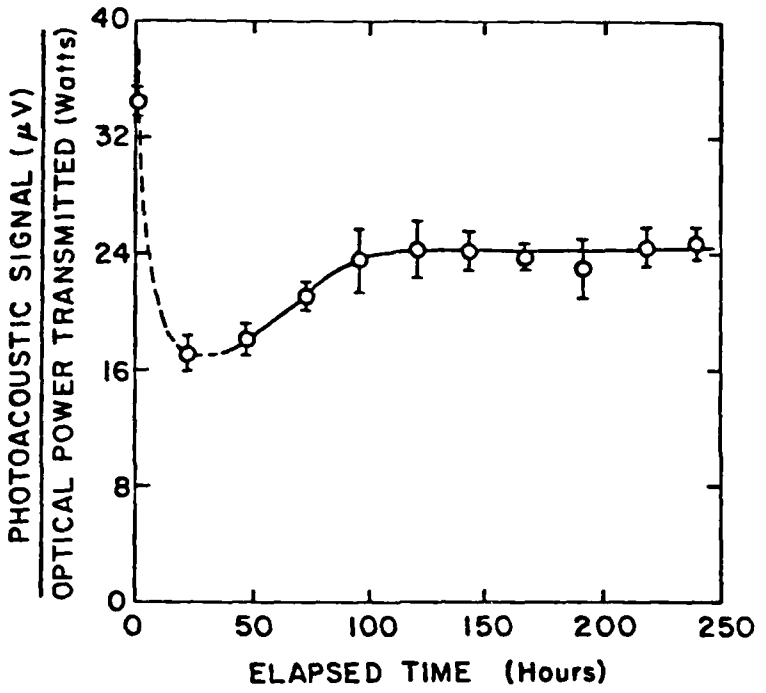

Figure 24

TIME DEPENDENCE OF PHOTOACOUSTIC SIGNAL DURING
WATER VAPOR EXPOSURE OF KCl CRYSTALS

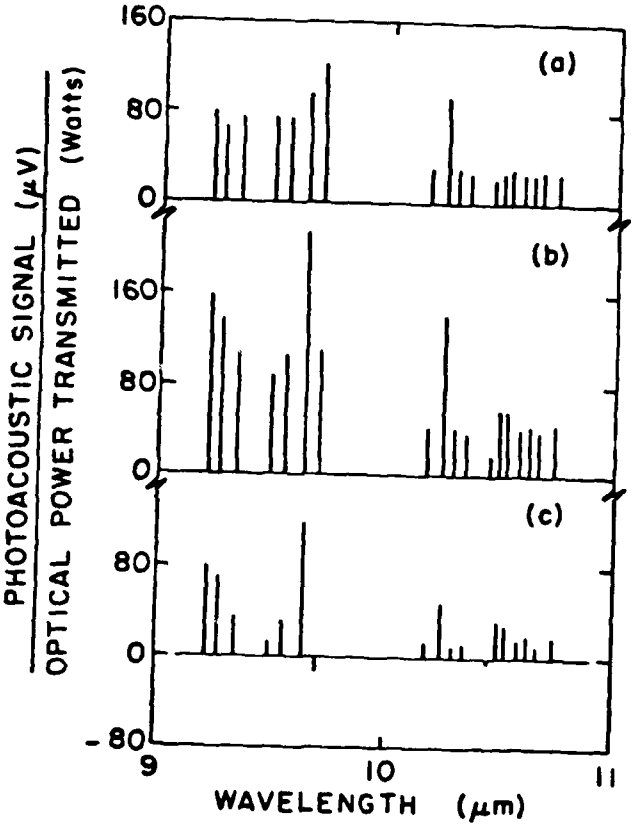

Figure 25

PHOTOACOUSTIC SPECTRA FOR KCl CRYSTALS (a) BEFORE VAPOR EXPOSURE, (b) AFTER VAPOR EXPOSURE, AND (c) DIFFERENCE SPECTRUM.

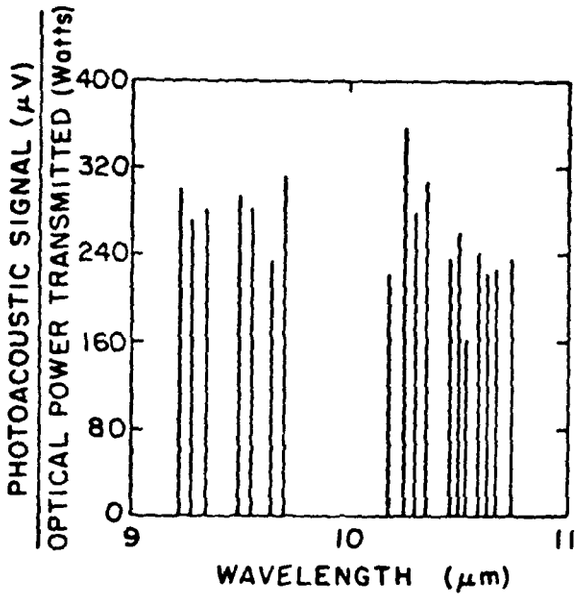

Figure 26

PHOTOACOUSTIC SPECTRUM FOLLOWING ATMOSPHERIC CONTAMINATION OF KCl CRYSTALS

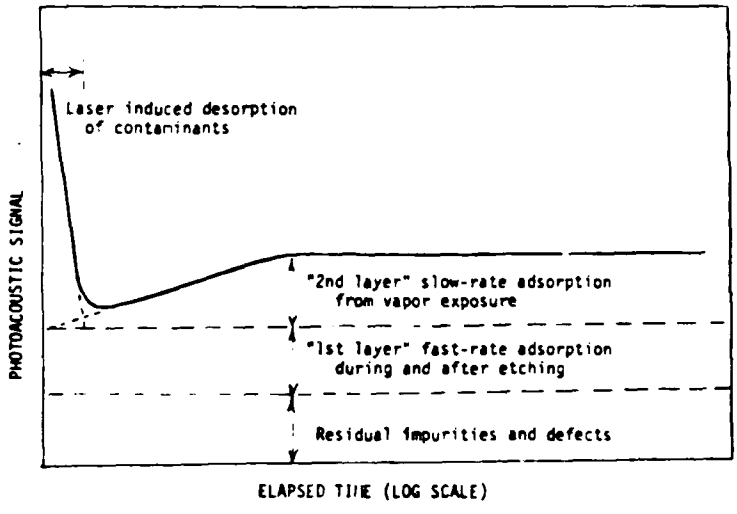

Figure 27

SCHEMATIC DIAGRAM OF TIME DEPENDENCE OF SURFACE ABSORPTANCE IN VAPOR EXPOSURE INVESTIGATION

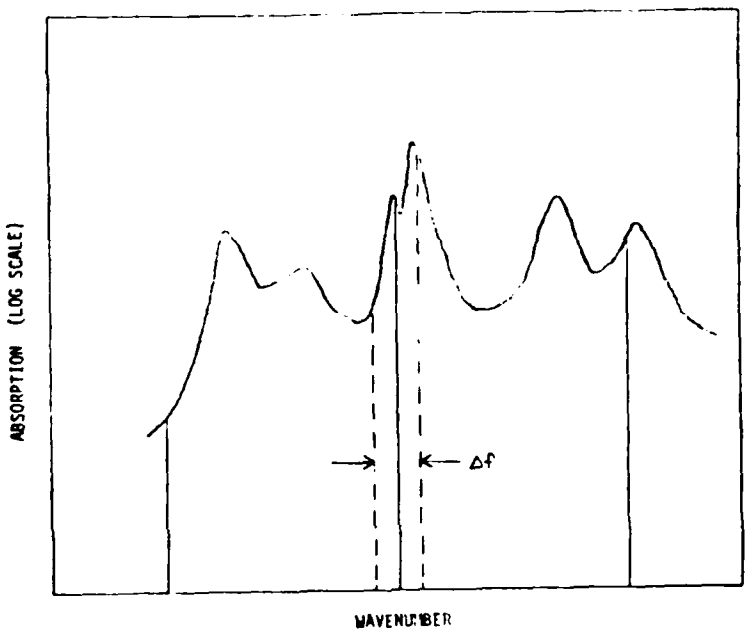

Figure 28

HYPOTHETICAL ABSORPTION SPECTRUM FOR SMALL GAS MOLECULES ADSORBED ON A TRANSPARENT CRYSTAL. SOLID VERTICAL LINES REPRESENT A FEW OF THE CO_2 LASER LINES AND DASHED VERTICAL LINES RERESENT THE FREQUENCY SCANNING TECHNIQUE FOR ONE OF THE CO_2 LASER LINES.

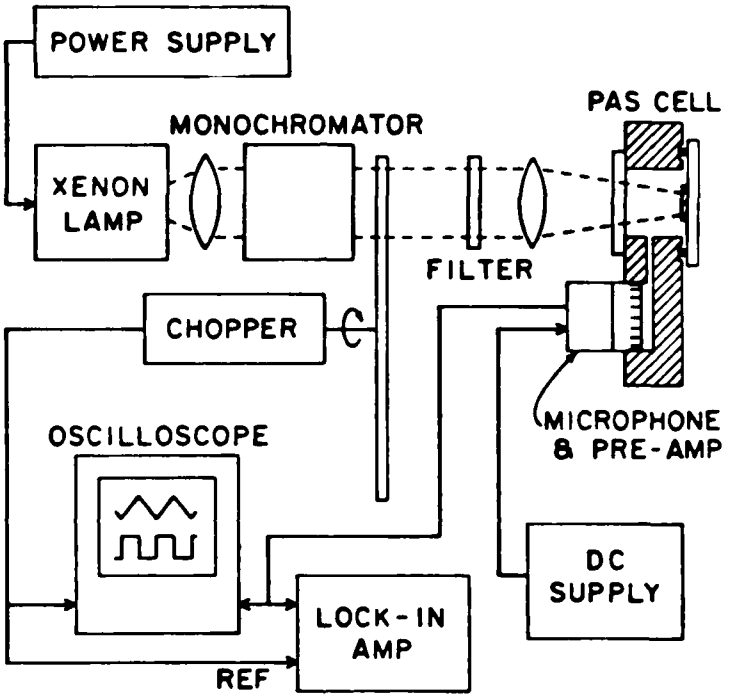

Figure 29

BLOCK DIAGRAM OF VISIBLE WAVELENGTH APPARATUS

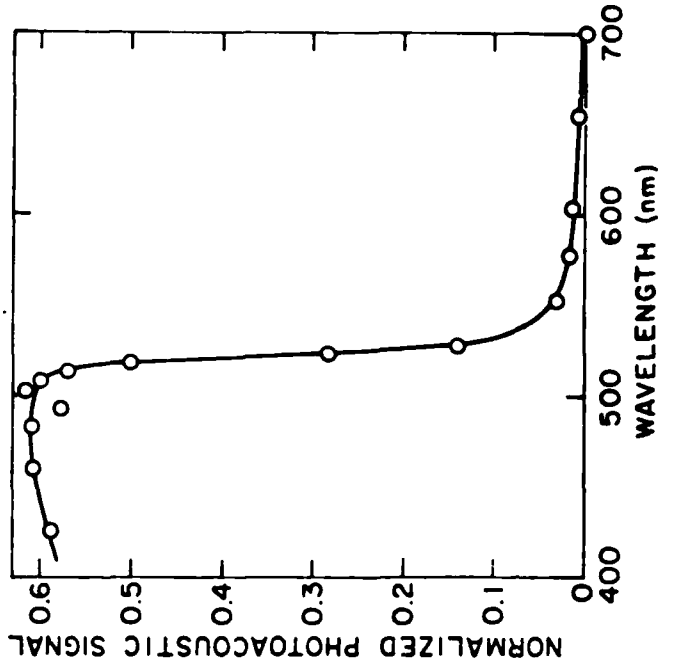

Figure 31

PHOTOACOUSTIC SPECTRUM FOR CdS CRYSTAL
(NORMALIZED TO FLAT-BLACK PAINT ON CdS)

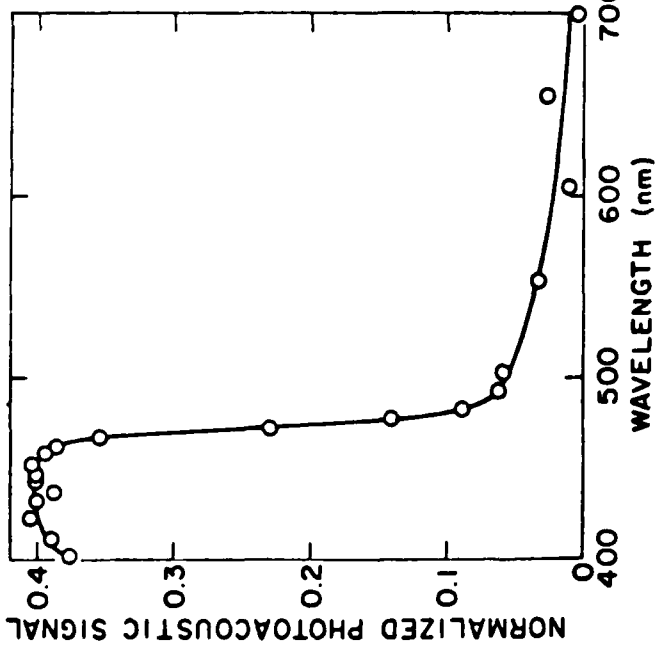

Figure 30

PHOTOACOUSTIC SPECTRUM OF ZnSe CRYSTAL
(NORMALIZED TO FLAT-BLACK PAINT ON ZnSe)

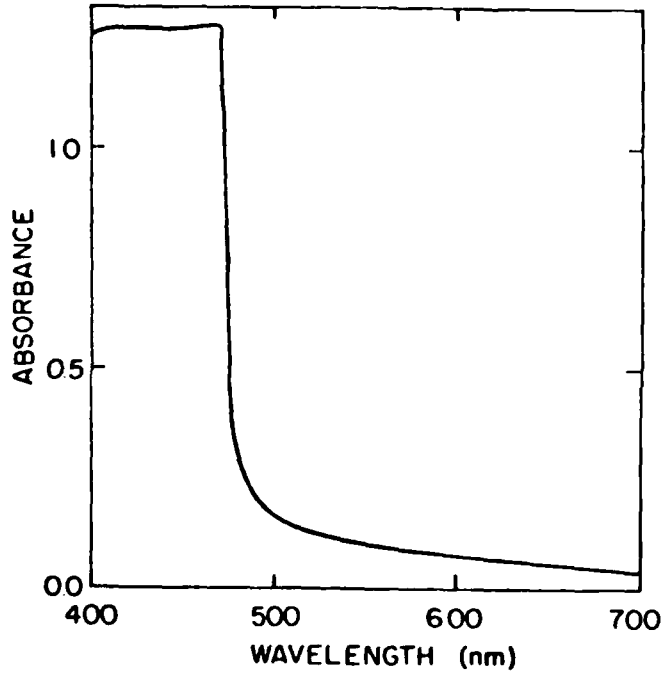

Figure 32

VISIBLE WAVELENGTH OPTICAL SPECTROMETER DATA
FOR ZnSe

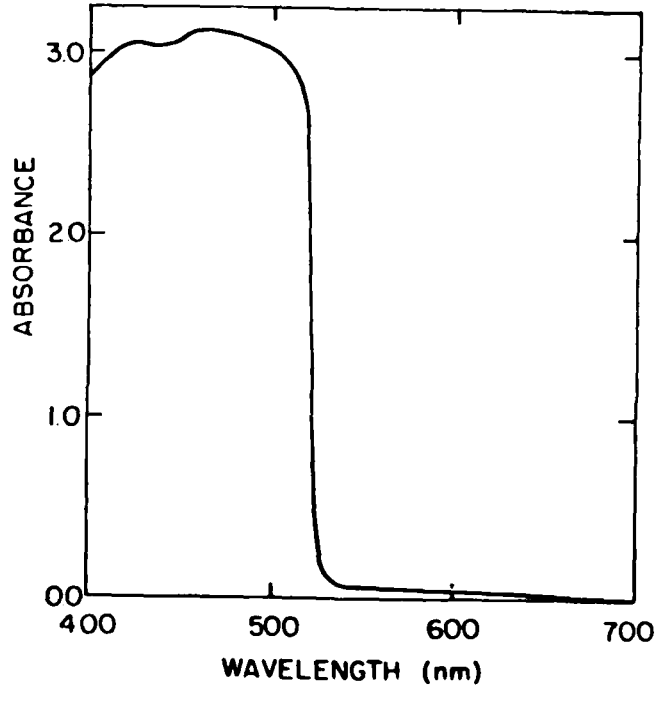

Figure 33

VISIBLE WAVELENGTH OPTICAL SPECTROMETER DATA
FOR CdS

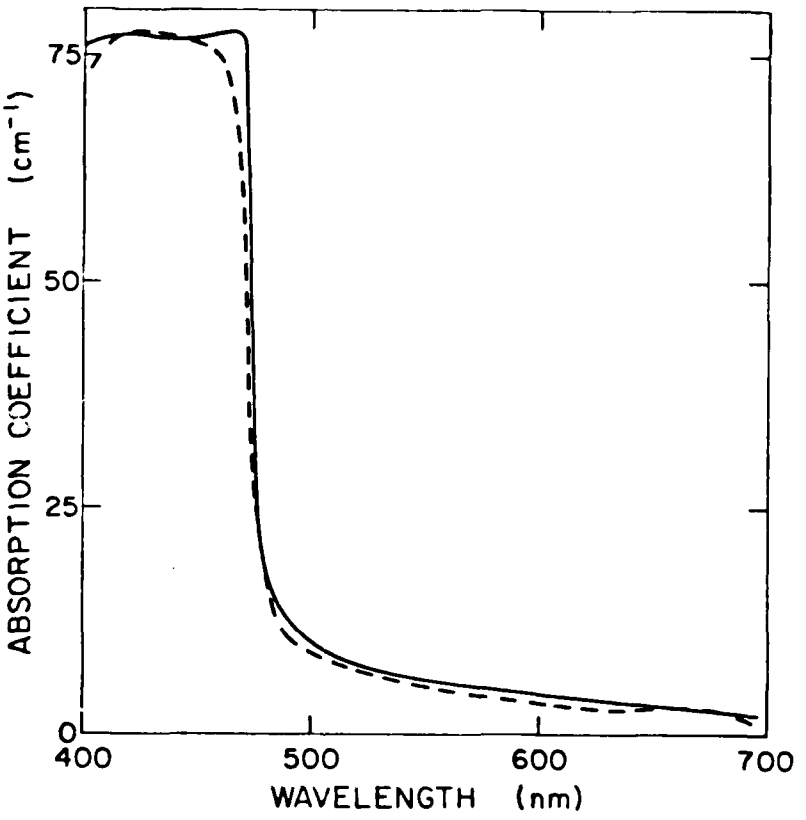

Figure 34

CALCULATED ABSORPTION COEFFICIENT USING OPTICAL DATA (SOLID LINE) AND PHOTOACOUSTIC DATA (DASHED LINE) FOR ZnSe

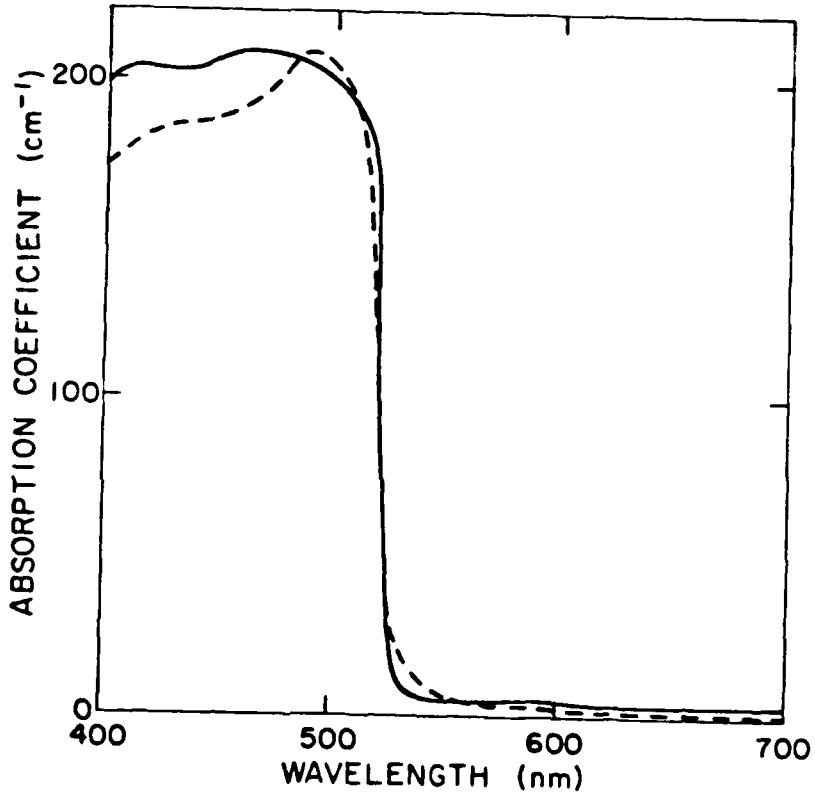

Figure 35

CALCULATED ABSORPTION COEFFICIENT USING OPTICAL DATA (SOLID LINE) AND PHOTOACOUSTIC DATA (DASHED LINE) FOR CdS


FILMED